8-1-2022

Exploration of New Physics in B to Dstar muon neutrino Using a New Monte Carlo Tool

Quinn Campagna

Exploration of New Physics in $\bar{B}^0 \to D^{*+}\ell^-\bar{\nu}$

Using a New Monte Carlo Tool

A Thesis
Submitted to the Faculty of
the University of Mississippi
in Partial Fulfillment of the Requirements
for the Degree of Master of Science
in High Energy Physics
in the Department of Physics and Astronomy

By
Quinn Campagna

Oxford, Mississippi

August 2022

ABSTRACT

Recent experimental results in B physics from Belle, BaBar and LHCb suggest new physics (NP) in the weak $b \to c$ charged-current and the $b \to s$ neutral-current processes. Here we focus on the charged-current case and specifically on the decay modes $\overline{B}^0 \to D^{*+}\ell^-\bar{\nu}$ with $\ell = e$ and μ. The world averages of the ratios R_D and R_D^* currently differ from the Standard Model (SM) predictions by 3.4σ while recently a new anomaly has been observed in the forward-backward asymmetry measurement, A_{FB}, in $\overline{B}^0 \to D^{*+}\mu^-\bar{\nu}$ decay. It is found that $\Delta A_{FB} = A_{FB}(B \to D^*\mu\nu) - A_{FB}(B \to D^*e\nu)$ is around 4.1σ away from the SM prediction in an analysis of 2019 Belle data. In this work we explore possible solutions to the ΔA_{FB} anomaly and point out correlated NP signals in other angular observables. These correlations between angular observables must be present in the case of beyond the Standard Model physics. We stress the importance of Δ type observables that are obtained by taking the difference of the observable for the muon and the electron mode. These quantities cancel form factor uncertainties in the SM and allow for clean tests of NP. These intriguing results also suggest an urgent need for improved simulation and analysis techniques in $\overline{B}^0 \to D^{*+}\ell^-\bar{\nu}$ decays. Here we also describe a new Monte Carlo Event-generator tool based on EVTGEN that we developed to allow simulation of the NP signatures in $\overline{B}^0 \to D^{*+}\ell^-\nu$, which arise due to the interference between the SM and NP amplitudes. We then discuss prospects for improved observables sensitive to NP couplings with 1, 5, 50, and 250 ab^{-1} of Belle II data, which seem to be ideally suited for this class of measurements.

ACKNOWLEDGEMENTS

This work was supported in part by NSF Grant No PHY-191514.

The findings and opinions in this thesis belong solely to the author, and are not necessarily those of the sponsor.

EvtGen was originally created by David Lange and Anders Ryd and is currently maintained by John Back, Michal Kreps, and Thomas Latham.

I thank my committee for their comments on this thesis, and I thank Dr. Alakabha Datta for directing this research.

I also thank Lopamudra Mukherjee, Bhubanjyoti Bhattacharya, Thomas E. Browder, Shawn Dubey, and Alexei Sibidanov for their collaboration on this work

TABLE OF CONTENTS

ACKNOWLEDGEMENTS iii

LIST OF TABLES vi

LIST OF FIGURES vii

CHAPTER

1. INTRODUCTION 1

    1.1 Motivation 2
    1.2 Angular Observables and Δ-Type Observables 4

2. THEORY 9

    2.1 Effective Field Theory Hamiltonian and Decay Amplitude 9
    2.2 Differential Decay Distributions 12

3. NEW-PHYSICS IMPLEMENTATION IN EVTGEN 15

4. SIGNATURES OF NEW PHYSICS 18

5. NEW-PHYSICS SENSITIVITY AND RESULTS 22

6. CONCLUSIONS 35

A. ANGULAR COEFFICIENTS 44

B. HELICITY AMPLITUDES AND FORM FACTORS 47

C. PARAMETERIZATIONS OF THE HADRONIC FORM FACTORS . . . 51

LIST OF TABLES

1.1 Possible NP Indications in $b \to c\tau\nu_\tau$ 3
4.1 Angular Observables and NP Dependences 20
5.1 Representative NP Scenarios 25
5.2 Integrated Δ Observable Predictions 29
B.1 Meson and Lepton Masses 50
C.1 CLN Parameters 53
C.2 HQET Parameters 62
C.3 Pole Masses of B_c resonances 63
C.4 BGL Input 63

LIST OF FIGURES

1.1 $\overline{B} \to D^*(\to D\pi)\ell^-\bar{\nu}$ Decay 8
5.1 Differential Distributions of $\overline{B} \to D^*\ell^-\bar{\nu}$ 23
5.2 Form Factor Uncertainties 24
5.3 Allowed Parameter Space 26
5.4 q^2 Distribution of Δ Observables 27
5.5 Statistical Uncertainties 30
5.6 Coarse-Binned Distributions 31
5.7 Correlations Between Angular Observables 33
C.1 Form Factor Parameterizations 61

CHAPTER 1

INTRODUCTION

The Standard Model (SM) is currently the most successful theory of particle physics. Its predictions have repeatedly been shown to be consistent with experimental measurements. However, the SM cannot be complete, as there are several natural phenomena which it does not describe, such as quantum gravity, dark matter, and dark energy. As such, one of the major goals of particle physics is to find physics beyond the SM.

One way to pursue this goal is to use high precision experiments to search for deviations from the SM. Because of the success of the SM, these potential deviations are generally expected to be small. However, they have the potential to point us in the direction of new physics (NP).

A powerful way to study physics beyond the SM is via virtual effects of new particles, not present in the SM, in low energy experiments. These virtual effects can in many cases probe mass scales beyond the reach of present or proposed colliders, where the new particles are expected to appear. There is also the possibility that beyond the Standard Model physics comes in the form of weakly coupled light new states. These new states are

more likely to be detected at low energy, high precision experiments. In this work we will focus on charged current semileptonic B decays, $\bar{B}^0 \to D^{*+}\ell^-\bar{\nu}$ with $\ell = e$ and μ. These decays originate from the underlying quark-level transitions $b \to c\ell^-\bar{\nu}_\ell$, where $\ell = e, \mu$, or τ. At the hadron level they manifest as decays such as $\bar{B} \to D^{(*)}\ell^-\bar{\nu}_\ell$.

1.1 Motivation

The charged-current decays $B \to D^{(*)}\tau\nu_\tau$ have been measured by the BaBar, Belle and LHCb experiments. Discrepancies with SM predictions of $R^{\tau\ell}_{D^{(*)}} \equiv \mathcal{B}(\overline{B} \to D^{(*)}\tau^-\bar{\nu}_\tau)/\mathcal{B}(\overline{B} \to D^{(*)}\ell^-\bar{\nu}_\ell)$ ($\ell = e, \mu$) [1–10] have been observed thus far. The SM predictions and the corresponding World-Averaged experimental results from the Heavy Flavor Averaging Group (HFLAV) [11] are shown in Table 1.1. The deviation from the SM in $R^{\tau\ell}_D$ and $R^{\tau\ell}_{D^*}$ (combined) has a significance of 3.4σ [12]. These measurements suggest the presence of NP that is lepton-flavor universality violating (LFUV) in $b \to c\tau\nu_\tau$ decays.

We will focus on the decay $\overline{B}^0 \to D^{*+}\ell^-\bar{\nu}$ as a laboratory to explore NP effects in $b \to c\ell^-\bar{\nu}_\ell$ transitions. At leading order, the $\overline{B}^0 \to D^{*+}\ell^-\bar{\nu}$ transitions proceed via the SM. However, new interactions can affect these decays at sub-leading orders. In experiment, the underlying transition is $b \to c\ell X$ where the invisible state X can be a left-handed (LH) neutrino (part of the SM LH doublet of leptons) or a light right-handed (RH) singlet neutrino. Here we will focus on NP scenarios that produce only LH neutrinos in the final state.

Observable	SM Prediction	Measurement (WA)
$R_{D^*}^{\tau/\ell}$	0.258 ± 0.005 [11]	$0.295 \pm 0.011 \pm 0.008$ [11]
$R_{D}^{\tau/\ell}$	0.299 ± 0.003 [11]	$0.340 \pm 0.027 \pm 0.013$ [11]
$R_{D^*}^{\mu/e}$	~ 1.0	$1.04 \pm 0.05 \pm 0.01$ [13]

Table 1.1: Measured values of observables that suggest NP in $b \to c\tau\nu_\tau$. Measurements presented in this table refer to World Averages (WA). Note that in [14], the most recent lattice data from [15] on $B \to D^*\ell\nu$ form factors were used to obtain the SM prediction for $R_{D^*}^{\tau/\ell}$, 0.2586 ± 0.0030.

Although the theoretical work on NP has concentrated on the semi-leptonic τ modes, where experimental statistics are limited, attention is now also being paid to the semi-leptonic muon and electron modes where data is plentiful. For example, scaling the Belle results in [16] to Belle II at 50 ab^{-1} we expect a yield of 8×10^6 events in each of the muon and electron modes. Similarly, scaling the BaBar results in [17] on $B \to D^*\ell\nu$ with a fully reconstructed hadronic tag, we expect 3×10^5 events with no background.

An additional advantage is that the missing neutrino momentum can be calculated from kinematic constraints of e^+e^- production at the $\Upsilon(4S)$ and the angular distributions can be fully reconstructed. Unlike the τ, which is detected through its decay products, the muon and electron are directly detected in experiment. In contrast, for semi-leptonic B decays to the τ lepton, the final state contains one or more additional neutrinos from the

τ decay, which complicates the situation. Examining NP in the muon mode is further motivated by the anomalous $(g-2)_\mu$ measurements [18] as well as by the neutral-current LFUV B anomalies in the $b \to s\mu^+\mu^-$ decays (see for example, Ref. [19]). At first glance, when studying the B anomalies within the framework of an Effective Field Theory (EFT), these anomalies may appear unrelated. However, within an SMEFT framework NP in the $b \to s\mu^+\mu^-$ transition could imply NP in the $b \to c\mu^-\bar{\nu}_\mu$ decay [20]. In this article, therefore, we will focus on the muon and electron modes, assuming that the electron decay mode is well described by the SM, but NP contributions are allowed in the muon mode.

1.2 Angular Observables and Δ-Type Observables

Although hints for NP have appeared in the ratio of rates such as $R_{D^{(*)}}$, establishing NP and diagnosing the type of NP will require examination of deviations from the SM in other observables as well. Several observables can be constructed from a complete differential distribution of events using helicity angles. Fig. 1.1 shows a schematic definition of the three helicity angles in $\overline{B} \to D^*(\to D\pi)\ell^-\bar{\nu}$.

Angular observables are even more interesting as these may provide one or more unambiguous signals for NP. One such sensitive angular observable is the forward-backward asymmetry of the charged lepton, A_{FB}, which can be reconstructed as the difference between the number of leptons with the lepton's helicity angle, θ_ℓ (see Fig. 1.1), greater and less than $\pi/2$. Another observable is S_3, which can be reconstructed as an asymmetric

integral over the angle χ, which measures the difference between the decay planes of the D^* and the lepton-neutrino system (see Fig. 1.1). There are additional interesting and correlated angular observables, such as S_5 and S_7, which require asymmetric integrals over multiple helicity angles. In Ref. [21], it was shown that NP in the μ modes can also be detected in the CP-violating triple-product terms, like S_7, in the angular distribution [22, 23].

A non-zero A_{FB} is present in both the muon and electron channels in the SM due to interference between different helicity amplitudes of the virtual W boson. However, in a Δ-type observable, $\Delta A_{FB} = A_{FB}^{\mu} - A_{FB}^{e}$, where one considers the difference between the muon and electron channels, the SM contributions approximately cancel, except for a small residual effect due to the dependence on the muon mass close to its threshold. Furthermore, we find that the observable ΔA_{FB} has reduced sensitivity to hadronic uncertainties in form factors. Therefore, any deviation from the SM prediction for ΔA_{FB} is likely due to NP effects. Recently, using the tables of Belle data from Ref. [16], an anomaly in ΔA_{FB} was reported in Ref. [24]. This could be a signature of LFUV NP [24–26].

LFUV NP in the electron and muon sectors is tightly constrained by the measurement of the ratio of rates $R_{D^{(*)}}^{\mu e} \equiv \mathcal{B}(\overline{B} \to D^{(*)}\mu^-\bar{\nu}_\mu)/\mathcal{B}(\overline{B} \to D^{(*)}e^-\bar{\nu}_e)$ which is 1.04 ± 0.05. We restrict ourselves to NP Scenarios in which a deviation of at most 3% from unity is allowed, which could be tested in the future. Even if the effects of LFUV NP are small in the ratios of decay rates, larger effects may be visible in the angular distributions.

In this thesis, I will discuss various solutions to explain the ΔA_{FB} anomaly. The framework used is based on a newly developed Monte Carlo (MC) event generator tool to simulate NP signatures in $B \to D^* \ell \nu$ in a realistic experimental environment. We employ our MC tool primarily to study semi-leptonic decays with a muon and electron in the final state. We assume that the electron decay mode is well described by the SM, but allow for NP contributions in the muon mode. Using this MC tool we generate results for three distinct scenarios with different NP couplings that are consistent with current data and can explain the ΔA_{FB} anomaly, while remaining consistent with other constraints. Furthermore, using MC simulations we demonstrate that Δ-type observables, such as ΔA_{FB} and ΔS_5, eliminate most QCD uncertainties from form factors and allow for clean measurements of NP. We introduce correlated observables that improve the sensitivity to NP. We also discuss prospects for improved observables sensitive to NP couplings with the expected 50 ab^{-1} of Belle II data, which seems to be ideally suited for this class of measurements. These measurements could also be possible at LHCb and other hadron collider experiments. We provide both integrated observables, for the benefit of current experimental analyses, and distributions of the observables as a function of q^2. We also suggest experimental requirements on q^2 and on laboratory lepton momenta to optimize sensitivity to NP and reduce systematics.

The layout of the remainder of this thesis is as follows. In Ch. 2, we discuss the theoretical basis of the full angular distribution for $\bar{B} \to D^* \ell^- \bar{\nu}$ in an effective theory framework. In Chs. 3, 4, and 5, we present the implementation of our NP MC tool, the signatures of and sensitivity to NP respectively. finally we conclude in Ch. 6.

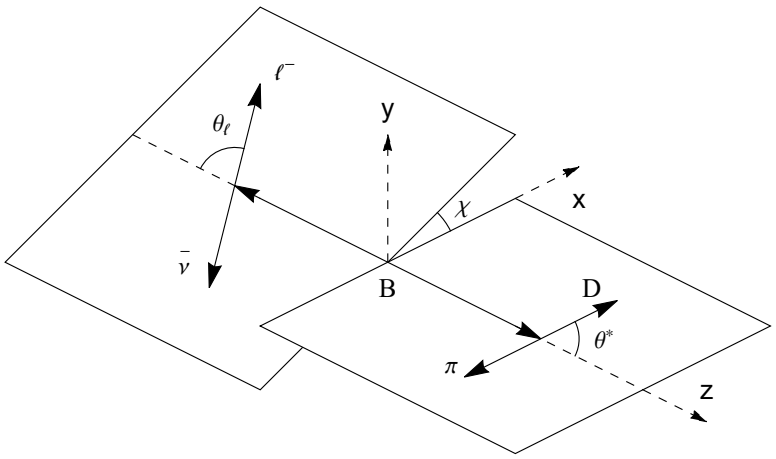

Figure 1.1: Schematic diagram defining various angles in $\overline{B} \to D^*(\to D\pi)\ell^-\bar{\nu}$ decay [21]. We have aligned the coordinate axes so that the decaying $\overline{B}$ meson is at rest at the origin and in this frame the momentum of the D^* meson is oriented along the z-axis. Subsequent decays are shown in the rest frames of the corresponding object that is decaying – $D^* \to D\pi$ is in the rest frame of the D^* and a virtual particle decays into $\ell^-\bar{\nu}$. The polar angles, θ^* and θ_ℓ, are respectively defined in these subsequent rest frames, while the azimuthal angle, χ, is defined in the rest frame of the $\overline{B}$ meson.

CHAPTER 2

THEORY

2.1 Effective Field Theory Hamiltonian and Decay Amplitude

In the study of NP in charged-current semi-leptonic B decays it is useful to adopt an EFT framework. In an EFT description of the $b \to c\ell^-\bar{\nu}$ decays, one writes down all possible dimension-six four-quark operators at the scale of the b-quark mass. The effective Hamiltonian that describes SM and NP effects can be expressed as,

$$\mathcal{H}_{\text{eff}} = \frac{G_F V_{cb}}{\sqrt{2}} \Big\{ [(1+g_L)\,\bar{c}\gamma_\alpha(1-\gamma_5)b + g_R\,\bar{c}\gamma_\alpha(1+\gamma_5)b]\,\bar{\mu}\gamma^\alpha(1-\gamma_5)\nu_\mu \\ + \; [g_S\,\bar{c}b + g_P\,\bar{c}\gamma_5 b]\,\bar{\mu}(1-\gamma_5)\nu_\mu + g_T\,\bar{c}\sigma^{\alpha\beta}(1-\gamma_5)b\bar{\mu}\sigma_{\alpha\beta}(1-\gamma_5)\nu_\mu \Big\} + h.c.\,, \tag{2.1}$$

where the factors g_X, $X = L, R, S, P,$ and T, are coupling constants that describe NP effects. As indicated earlier, we have only included LH neutrinos in this EFT, however, we have allowed for both LH and RH NP couplings.

Based on the effective Hamiltonian of Eq. (2.1), one can express the decay amplitude for the process $\overline{B} \to D^*(\to D\pi)\ell\bar{\nu}$ as [21, 27],

$$\mathcal{M} = \frac{4\,G_F V_{cb}}{\sqrt{2}} \Bigg\{ \left\langle D\pi \left| \bar{c}\gamma^\mu \left[(1+g_L)P_L + g_R P_R\right] b \right| \overline{B} \right\rangle (\bar{\ell}\gamma_\mu P_L \nu)$$

$$+ \left\langle D\pi \left| \bar{c} \left(g_{S_L} P_L + g_{S_R} P_R \right) b \right| \overline{B} \right\rangle (\bar{\ell} P_L \nu) + g_T \left\langle D\pi \left| \bar{c} \sigma^{\mu\nu} b \right| \overline{B} \right\rangle (\bar{\ell} \sigma_{\mu\nu} P_L \nu) \Bigg\}, \tag{2.2}$$

where $P_{R,L} = (1 \pm \gamma_5)/2$. This decay amplitude contains several hadronic matrix elements that describe the $\overline{B} \to D^* \to D\pi$ transitions through LH and RH scalar and vector currents, as well as a tensor current. The $D^* \to D\pi$ decay is mediated solely by the strong force, so that

$$\langle D\pi | D^*(k,\epsilon) \rangle \;\; = \;\; \epsilon \cdot (p_D - p_\pi), \tag{2.3}$$

where $p_{D(\pi)}$ is the four-momentum of the $D(\pi)$, $k = p_D + p_\pi$ is the four-momentum of the D^* and ϵ is its polarization. Note that these satisfy the on-shell condition $k \cdot \epsilon = 0$.

The remaining parts of the hadronic matrix elements that appear in Eq. (2.2) are [28]:

$$\left\langle D^*(k,\epsilon) \left| \bar{c} \gamma_\mu b \right| \overline{B}(p) \right\rangle = -i \varepsilon_{\mu\nu\rho\sigma} \epsilon^{*\nu} p^\rho k^\sigma \frac{2V(q^2)}{m_B + m_{D^*}}, \tag{2.4}$$

$$\begin{aligned} \left\langle D^*(k,\epsilon) \left| \bar{c} \gamma_\mu \gamma^5 b \right| \overline{B}(p) \right\rangle = {} & \epsilon_\mu^* (m_B + m_{D^*}) A_1(q^2) - (p+k)_\mu (\epsilon^* \cdot q) \frac{A_2(q^2)}{m_B + m_{D^*}} \\ & - \; q_\mu (\epsilon^* \cdot q) \frac{2 m_{D^*}}{q^2} [A_3(q^2) - A_0(q^2)], \end{aligned} \tag{2.5}$$

$$\left\langle D^*(k,\epsilon) \left| \bar{c} \gamma^5 b \right| \overline{B}(p) \right\rangle = -(\epsilon^* \cdot q) \frac{2 m_{D^*}}{m_b + m_c} A_0(q^2), \tag{2.6}$$

$$\begin{aligned} \left\langle D^*(k,\epsilon) \left| \bar{c} \sigma_{\mu\nu} b \right| \overline{B}(p) \right\rangle = \varepsilon_{\mu\nu\rho\sigma} \Bigg\{ & -\epsilon^{\rho *} (p+k)^\sigma T_1(q^2) + \epsilon^{\rho *} q^\sigma \frac{m_B^2 - m_{D^*}^2}{q^2} [T_1(q^2) - T_2(q^2)] \\ & + 2 \frac{\epsilon^* \cdot q}{q^2} p^\rho k^\sigma \left[T_1(q^2) - T_2(q^2) - \frac{q^2}{m_B^2 - m_{D^*}^2} T_3(q^2) \right] \Bigg\} \end{aligned} \tag{2.7}$$

where p is the four-momentum of the B meson, q represents the four-momentum of the lepton-neutrino pair, while $m_{B(D^*)}$ represents the mass of the $B(D^*)$ meson. Here, V, A_0, A_1, A_2, A_3, T_1, T_2 and T_3 are the relevant form factors for a $\overline{B} \to V$ transition, the explicit forms of which are given in Appendix B. For the Levi-Civita tensor, $\varepsilon_{\mu\nu\rho\sigma}$, we use the convention $\varepsilon_{0123} = +1$.

For easy comparison with similar literature in the field, below we present an alternative notation and its connection to the notation used in this article. Following the presentation in Ref. [24], the effective Lagrangian that describes $b \to c\ell^-\bar{\nu}$ transitions can be written as

$$\mathcal{L} \;=\; -\frac{4G_F}{\sqrt{2}} \sum_i C_i \mathcal{O}_i + h.c. \,, \tag{2.8}$$

where $i = V_L, V_R, S_L, S_R$, and T, and C_i represents the Wilson Coefficient (WC) corresponding to the operator $\mathcal{O}_i$. Note the negative sign added to this Lagrangian in order to obtain the correct sign for the SM term (see for example Eq. (20.90) in [29] with errata in [30]). The WC's can be easily converted into the NP coupling constants that appear in Eq. (2.1) as follows.

$$C_{V_L} \;=\; 1 + g_L \,, \;\; C_{V_R} \;=\; g_R \,, \;\; C_{S_L} \;=\; g_S - g_P \,, \;\; C_{S_R} \;=\; g_S + g_P \,, \;\; C_T \;=\; g_T \,. \tag{2.9}$$

Note that only C_{V_L} has both SM and NP parts while all other WCs are NP only. Furthermore, for a $\overline{B} \to V$ transition, where V denotes a vector meson, the scalar matrix element $\langle V|\bar{q}b|B\rangle = 0$. As a consequence, the following condition must be imposed,

$$C_{S_R} + C_{S_L} \;=\; 2\, g_S \;=\; 0\,. \tag{2.10}$$

Thus, there are only four independent NP parameters that can be used to describe the decay $\overline{B} \to D^*\ell^-\bar{\nu}$ process, namely g_L, g_R, g_P, and g_T. We will use the g_i parameters to describe the results and plots presented in this article.

2.2 Differential Decay Distributions

One can now express the differential decay distribution for $\overline{B} \to D^*(\to D\pi)\ell^-\bar{\nu}$ as a function of four kinematic variables – q^2 and three helicity angles θ^*, θ_ℓ, and χ (see Fig. 1.1 for a schematic diagram defining these angles) – in the following form.

$$\begin{aligned}
\frac{d^4\Gamma}{dq^2\, d\cos\theta^*\, d\cos\theta_\ell\, d\chi} \;=\; \frac{9}{32\pi}\Big[&\left(I_1^s \sin^2\theta^* + I_1^c \cos^2\theta^*\right) + \left(I_2^s \sin^2\theta^* + I_2^c \cos^2\theta^*\right)\cos 2\theta_\ell \\
&+ I_3 \sin^2\theta^* \sin^2\theta_\ell \cos 2\chi + I_4 \sin 2\theta^* \sin 2\theta_\ell \cos\chi \\
&+ I_5 \sin 2\theta^* \sin\theta_\ell \cos\chi + \left(I_6^c \cos^2\theta^* + I_6^s \sin^2\theta^*\right)\cos\theta_\ell \\
&+ I_7 \sin 2\theta^* \sin\theta_\ell \sin\chi + I_8 \sin 2\theta^* \sin 2\theta_\ell \sin\chi \\
&+ I_9 \sin^2\theta^* \sin^2\theta_\ell \sin 2\chi\Big]\,,
\end{aligned} \tag{2.11}$$

where the 12 coefficients $I_i^{(s,c)}(q^2)$ (i = 1,...,9) can be expressed in terms of eight helicity amplitudes that in turn depend on the NP parameters g_L, g_R, g_P, and g_T. For brevity, the ex-

act dependence of the coefficient functions, $I_i^{(s,c)}$ is given in Appendix A. The distribution for the CP-conjugate process is obtained with the following transformation, $\theta_l \to \pi - \theta_l$ and $\chi \to \pi + \chi$. The various helicity amplitudes transform as $\mathcal{A}_{SP} \to -\bar{\mathcal{A}}_{SP},\ \mathcal{A}_t \to -\bar{\mathcal{A}}_t,\ \mathcal{A}_{0(,T)} \to \bar{\mathcal{A}}_{0(,T)},\ \mathcal{A}_{||(,T)} \to \bar{\mathcal{A}}_{||(,T)},\ \mathcal{A}_{\perp(,T)} \to -\bar{\mathcal{A}}_{\perp(,T)} (\mathcal{A}_{\pm(,T)} \to \bar{\mathcal{A}}_{\mp(,T)})$ leading to the angular coefficients transformations $I^{(a)}_{1,2,3,4,7} \to \bar{I}^{(a)}_{1,2,3,4,7}$ and $I^{(a)}_{5,6,8,9} \to -\bar{I}^{(a)}_{5,6,8,9}$[1]. Note that if one writes $\mathcal{A} = |A|e^{i\phi+i\delta}$, then $\bar{\mathcal{A}} = |A|e^{-i\phi+i\delta}$, where ϕ is the CP violating weak phase and δ is the CP conserving strong phase.

The full phase space for the $\overline{B} \to D^*\ell^-\bar{\nu}$ decay is obtained by varying the kinematic variables over their allowed ranges which are as follows: $m_\ell^2 \le q^2 \le m_B^2 - m_{D^*}^2, 0 \le \theta_{D^*,\ell} \le \pi$, and $0 \le \chi \le 2\pi$. One can now construct several observables by integrating the distribution of Eq. (2.11) over one or more of these kinematic variables. The first of these is the differential decay distribution as a function of q^2, constructed by integrating over the full range of allowed values for all three helicity angles.

$$\frac{d\Gamma}{dq^2} = \frac{1}{4}\left[3\, I_1^c - I_2^c + 2\left(3\, I_1^s - I_2^s\right)\right]. \tag{2.12}$$

[1]Our convention is similar to the LHCb convention for the $B^0 \to K^{*0}\ell^+\ell^-$ decay where θ_ℓ is defined as the angle between $K^{*0}(\bar{K}^{*0})$ and $\mu^+(\mu^-)$ for the $B^0(\overline{B}^0)$ decay leading to the transformations $I^{(a)}_{1,2,3,4,5,6} \to \bar{I}^{(a)}_{1,2,3,4,5,6}$ and $I_{7,8,9} \to -\bar{I}_{7,8,9}$ for CP conjugation with $\chi \to 2\pi - \chi$ [31]. Alternatively, when θ_ℓ is defined as the angle between $K^{*0}(\bar{K}^{*0})$ and the lepton ℓ^- for the $B^0(\overline{B}^0)$ decay while χ is the angle between the $K^\pm\pi^\mp$ and the $\ell^+\ell^-$ planes in both cases, the angular coefficients transform as $I^{(a)}_{1,2,3,4,7} \to \bar{I}^{(a)}_{1,2,3,4,7}$ and $I^{(a)}_{5,6,8,9} \to -\bar{I}^{(a)}_{5,6,8,9}$ for the CP conjugate process with $\theta_\ell \to \theta_\ell - \pi$ and $\chi \to -\chi$ [32, 33]. Note that, in all of these conventions, including ours, the $\frac{d^4(\Gamma+\bar{\Gamma})}{dq^2 d\cos\theta^* d\cos\theta_\ell d\chi}$ distribution for the untagged decay retains the contribution from the "true" CP violating terms [34, 35].

Next, one can construct double-differential decay distributions as functions of q^2 and one other angle variable at a time, obtained by integrating over the other two angles.

$$\frac{d^2\Gamma}{dq^2 d\cos\theta^*} = \frac{3}{4}\frac{d\Gamma}{dq^2}\left[2\,F_L^{D^*}(q^2)\cos^2\theta^* + F_T^{D^*}(q^2)\sin^2\theta^*\right], \tag{2.13}$$

$$\frac{d^2\Gamma}{dq^2 d\cos\theta_\ell} = \frac{d\Gamma}{dq^2}\left(\frac{1}{2} + A_{FB}\,\cos\theta_\ell + \frac{1-3\,\tilde{F}_L^\ell}{4}\,\frac{3\,\cos^2\theta_\ell - 1}{2}\right), \tag{2.14}$$

$$\frac{d^2\Gamma}{dq^2 d\chi} = \frac{1}{2\pi}\frac{d\Gamma}{dq^2}\left(1 + S_3\,\cos 2\chi + S_9\,\sin 2\chi\right), \tag{2.15}$$

where $F_{L(T)}^{D^*}(q^2)$ is the longitudinal (transverse) polarization of the D^*, A_{FB} is the charged-lepton forward-backward asymmetry, and S_9 is a triple-product asymmetry. The coefficient functions that appear in Eq. (2.15) can be expressed in terms of the angular coefficients, $I_i^{(s,c)}$, as follows.

$$F_L^{D^*}(q^2) = 1 - F_T^{D^*}(q^2) = \frac{3\,I_1^c - I_2^c}{3\,I_1^c - I_2^c + 2\,(3\,I_1^s - I_2^s)}, \tag{2.16}$$

$$A_{FB}(q^2) = \frac{3}{2}\,\frac{2\,I_6^s + I_6^c}{3\,I_1^c - I_2^c + 2\,(3\,I_1^s - I_2^s)}, \tag{2.17}$$

$$\tilde{F}_L^\ell(q^2) = \frac{I_1^c - 3\,I_2^c + 2(I_1^s - 3\,I_2^s)}{3\,I_1^c - I_2^c + 2\,(3\,I_1^s - I_2^s)}, \tag{2.18}$$

$$S_3(q^2) = \frac{4\,I_3}{3\,I_1^c - I_2^c + 2\,(3\,I_1^s - I_2^s)}, \tag{2.19}$$

$$S_9(q^2) = \frac{4\,I_9}{3\,I_1^c - I_2^c + 2\,(3\,I_1^s - I_2^s)}. \tag{2.20}$$

Note that there are additional observables that can be extracted from data by performing asymmetric integrals over more than one angles. We discuss some such observables in Section 4.

CHAPTER 3

NEW-PHYSICS IMPLEMENTATION IN EVTGEN

We implement the preceding discussion in the EvtGen MC simulation framework [36] as the new BTODSTARLNUNP decay model. This NP generator, BTODSTARLNUNP, can run either in a standalone mode or be integrated into a software framework of a B-physics experiment. The model includes SM contributions, various NP parameters as well as their interference. The model takes the NP parameters $\delta C_{V_L} \equiv g_L$, C_{V_R}, C_{S_L}, C_{S_R}, and C_T as inputs. The user specifies the NP parameters keeping in mind that the scalar coefficients (C_{S_L}, C_{S_R}) are related to each other by Eq. (2.10). Each of these parameters can take complex values as inputs and are entered in the user decay file. The default value for each parameter has been set to zero so that when no value is specified for these parameters the code returns SM results. Below we present an example of a user decay file to illustrate the usage of the NP MC generator.

```
## first argument is cartesian(0) or polar(1) representation of NP
## coefficients which are three consecutive numbers
## {id, Re(C), Im(C)} or {id, |C|, Arg(C)}
## id==0 \delta C_VL -- left-handed vector coefficient change from SM
```

```
## id==1 C_VR -- right-handed vector coefficient

## id==2 C_SL -- left-handed scalar coefficient

## id==3 C_SR -- right-handed scalar coefficient

## id==4 C_T  -- tensor coefficient


Decay B0

## B0 -> D*- e+ nu_e is generated with the Standard Model only

1   D*-    e+   nu_e   BTODSTARLNUNP;

Enddecay


Decay anti-B0

## anti-B0 -> D*+ mu- anti-nu_mu is generated

## with the addition of New Physics

1 D*+  mu-  anti-nu_mu  BTODSTARLNUNP 0 0 0.06 0 1 0.075 0 2 0 -0.2 3 0 0.2;

Enddecay


End
```

To generate NP the user inputs several arguments in the user decay file. The first of these specifies whether the remaining arguments are to be entered in Cartesian (0) or polar (1) coordinate system. Next, the user enters sets of three values. The first specifies the

type of NP coupling ($\delta C_{V_L}, C_{V_R}, C_{S_L}, C_{S_R}$, and C_T), while the second and third represent the real and imaginary parts in Cartesian coordinates, or magnitude and complex phase in polar coordinates. In the above example we have shown how the user can generate events for the SM as well as for a specific NP scenario which in our case is NP scenario 2. A complete version of the NP MC tool with an implementation of the BTODSTARLNUNP decay model can be found in Ref. [37].

CHAPTER 4

SIGNATURES OF NEW PHYSICS

The ratios of branching fractions as well as the differential q^2 distributions have limited sensitivity to NP for $b \to c\ell\nu$, $\ell = e, \mu$, which receive tree-level contributions in the SM and are hence unsuppressed. In contrast, angular observables have much better sensitivity to the interference between SM and NP. The optimal sensitivity to NP can be obtained by studying these angular observables as functions of q^2. We will examine four angular asymmetries as functions of q^2 to make predictions for our NP scenarios, A_{FB}, S_3, S_5, and S_7. A_{FB} and S_3 are previously defined in Section 2, while S_5 and S_7 are the coefficients of $\sin\theta_\ell \sin 2\theta^* \cos\chi$ and $\sin\theta_\ell \sin 2\theta^* \sin\chi$, respectively. These asymmetries can be constructed from the full angular distribution of Eq. (2.11) through asymmetric integrals shown below.

$$A_{FB}(q^2) = \left(\frac{d\Gamma}{dq^2}\right)^{-1} \left[\int_0^1 - \int_{-1}^0\right] d\cos\theta_\ell \, \frac{d^2\Gamma}{d\cos\theta_\ell dq^2}, \tag{4.1}$$

$$S_3(q^2) = \left(\frac{d\Gamma}{dq^2}\right)^{-1} \left[\int_0^{\pi/4} - \int_{\pi/4}^{\pi/2} - \int_{\pi/2}^{3\pi/4} + \int_{3\pi/4}^{\pi} + \int_{\pi}^{5\pi/4} - \int_{5\pi/4}^{3\pi/2} - \int_{3\pi/2}^{7\pi/4} + \int_{7\pi/4}^{2\pi}\right] d\chi \, \frac{d^2\Gamma}{dq^2 d\chi}, \tag{4.2}$$

$$S_5(q^2) = \left(\frac{d\Gamma}{dq^2}\right)^{-1} \left[\int_0^{\pi/2} - \int_{\pi/2}^{\pi} - \int_{\pi}^{3\pi/2} + \int_{3\pi/2}^{2\pi}\right] d\chi \left[\int_0^{1} - \int_{-1}^{0}\right] d\cos\theta^* \, \frac{d^3\Gamma}{dq^2 d\cos\theta^* d\chi}, \tag{4.3}$$

$$S_7(q^2) = \left(\frac{d\Gamma}{dq^2}\right)^{-1} \left[\int_0^{\pi} - \int_{\pi}^{2\pi}\right] d\chi \left[\int_0^{1} - \int_{-1}^{0}\right] d\cos\theta^* \, \frac{d^3\Gamma}{dq^2 d\cos\theta^* d\chi} \, . \tag{4.4}$$

To extract these asymmetries from data, we calculate the integrals in Eqs. (4.1-4.4) from binned distributions of the appropriate angular variables. For example, consider S_5. This distribution involves asymmetric integrals over both $\cos\theta^*$ and χ. For a given bin of q^2, we first divide the events into χ bins of size $\pi/2$. In each of these bins, we then divide the events into $\cos\theta^*$ bins of size 1. This gives us 8 bins corresponding to the various terms of Eq. (4.3), which we will label N_i with $i = 1, 2, ..., 8$. To find the value of S_5 for a given q^2 bin, we then combine the N_i's in the same way as the integrals in Eq. (4.3), normalized by $\sum_{i=1}^{8} N_i$.

When generating our predictions, we used $\Delta A_{FB} = A_{FB}(B \to D^* \mu\nu) - A_{FB}(B \to D^* e\nu)$, $\Delta S_3 = S_3(B \to D^* \mu\nu) - S_3(B \to D^* e\nu)$, and $\Delta S_5 = S_5(B \to D^* \mu\nu) - S_5(B \to D^* e\nu)$, where the electron mode has been generated with the SM only while the muon mode contains both SM and NP contributions. These are Δ-type observables

Observable	Angular Function	NP Dependence	m_ℓ suppression order
A_{FB}	$\cos\theta_\ell$	$\mathrm{Re}\,[g_T g_P^*]$ $\mathrm{Re}\,[(1+g_L-g_R)(1+g_L+g_R)^*]$	$\mathcal{O}(1)$
		$\mathrm{Re}\,[(1+g_L-g_R)g_P^*]$ $\mathrm{Re}\,[g_T(1+g_L-g_R)^*]$ $\mathrm{Re}\,[g_T(1+g_L+g_R)^*]$	$\mathcal{O}(m_\ell/\sqrt{q^2})$
		$\lvert 1+g_L-g_R\rvert^2$ $\lvert g_T\rvert^2$	$\mathcal{O}(m_\ell^2/q^2)$
S_3	$\sin^2\theta^*\sin^2\theta_\ell\cos 2\chi$	$\lvert 1+g_L+g_R\rvert^2$ $\lvert 1+g_L-g_R\rvert^2$ $\lvert g_T\rvert^2$	$\mathcal{O}(1),\ \mathcal{O}(m_\ell^2/q^2)$
S_5	$\sin 2\theta^*\sin\theta_\ell\cos\chi$	$\mathrm{Re}\,[g_T g_P^*]$	$\mathcal{O}(1)$
		$\lvert 1+g_L-g_R\rvert^2$	$\mathcal{O}(1),\ \mathcal{O}(m_\ell^2/q^2)$
		$\mathrm{Re}\,[(1+g_L-g_R)g_P^*]$ $\mathrm{Re}\,[g_T(1+g_L-g_R)^*]$ $\mathrm{Re}\,[g_T(1+g_L+g_R)^*]$	$\mathcal{O}(m_\ell/\sqrt{q^2})$
		$\lvert g_T\rvert^2$	$\mathcal{O}(m_\ell^2/q^2)$
S_7	$\sin 2\theta^*\sin\theta_\ell\sin\chi$	$\mathrm{Im}\,[g_P g_T^*]$	$\mathcal{O}(1)$
		$\mathrm{Im}\,[(1+g_L+g_R)g_P^*]$ $\mathrm{Im}\,[(1+g_L-g_R)g_T^*]$	$\mathcal{O}(m_\ell/\sqrt{q^2})$
		$\mathrm{Im}\,[(1+g_L-g_R)(1+g_L+g_R)^*]$	$\mathcal{O}(m_\ell^2/q^2)$

Table 4.1: Angular functions corresponding to angular observables A_{FB}, S_3, S_5, and S_7 alongside NP parameters that contribute to each. The dependence on NP parameters has been separated into different orders of $m_\ell/\sqrt{q^2}$.

as defined above, which eliminate most of the QCD uncertainties in the form factors, allowing for a clean measurement of LFUV NP. The asymmetry S_7 is always zero in the SM, and therefore was not recast into the form of a Δ observable. The NP dependences of A_{FB}, S_3, S_5, and S_7 are given in Table 4.1. Note that these dependencies have different weights, which are dependent on q^2. For all theory plots presented here, we have only used uncorrelated central values of the FF parameters as listed in Tables. C.1 and C.2. We verify that the Δ variables have minimal dependence on form factors. As a test, we consider CLN [38], BGL [39], and HQET [40] form factors. There are also other form factor models [41, 42]. Unless otherwise stated, we use the CLN parameterization of the hadronic form factors as the default in our predictions.

CHAPTER 5

NEW-PHYSICS SENSITIVITY AND RESULTS

The q^2 distribution alone has little sensitivity to NP, as shown in Fig. 5.1. On the other hand, angular asymmetries as functions of q^2 are quite sensitive to NP couplings. In particular, the angular asymmetries in the angle θ_ℓ and χ can be promising probes of NP as shown in Fig. 5.1. However, the angular asymmetries remain quite sensitive to form-factor uncertainties. As an example, in Fig. 5.2, the uncertainty in the predictions for A_{FB}^{μ} in the SM with four different form-factor parameterizations is shown. To address this issue we consider differences between angular asymmetries in the muon and electron channels using Δ observables. As one observes in Fig. 5.2, using ΔA_{FB} as an example, the predictions of the Δ observables are robust against form-factor uncertainties. In the SM the form-factor uncertainties cancel effectively in the Δ observables while with NP the cancellation is slightly less effective, since the NP violates lepton universality.

From our initial scan, we cannot reproduce the experimental ΔA_{FB} anomaly with a single NP coupling. Instead, we consider scenarios with several NP couplings. In order to match ΔA_{FB} from Ref. [24], we require a g_R NP coupling. In order to maintain the LFU

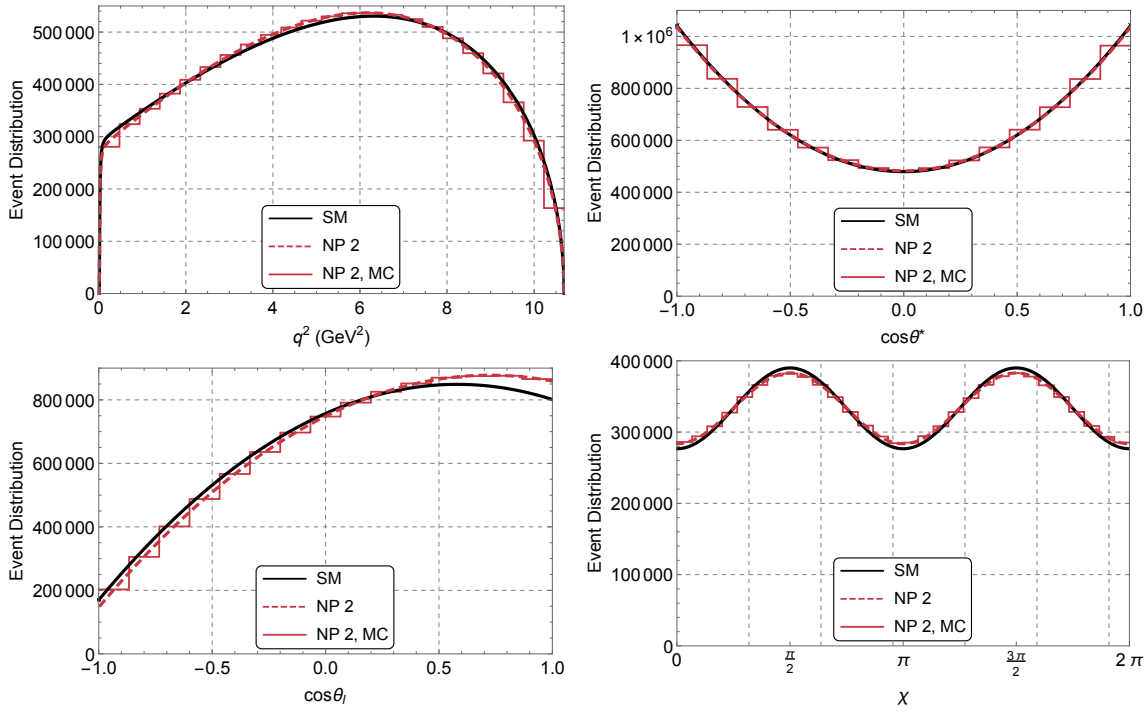

Figure 5.1: Distribution of $\overline{B} \to D^* \ell^- \bar{\nu}$ events as functions of (clockwise from top left) q^2, $\cos\theta^*$, χ, and $\cos\theta_\ell$. Theory predictions are shown for the SM (solid black curve) and for NP Scenario 2 (dashed red curve). EvtGen data are shown for NP Scenario 2 (solid red histogram). Each plot is fully integrated over three of the four kinematic variables. The q^2 range is divided into 23 equal bins, to reflect the expected resolution of experimental measurements. The angular bins are chosen to be sufficiently fine to compare MC data to the theory. The $\cos\theta$ ranges are divided into 15 equal bins, and the χ range, being twice as large as the θ ranges, is divided into twice as many bins.

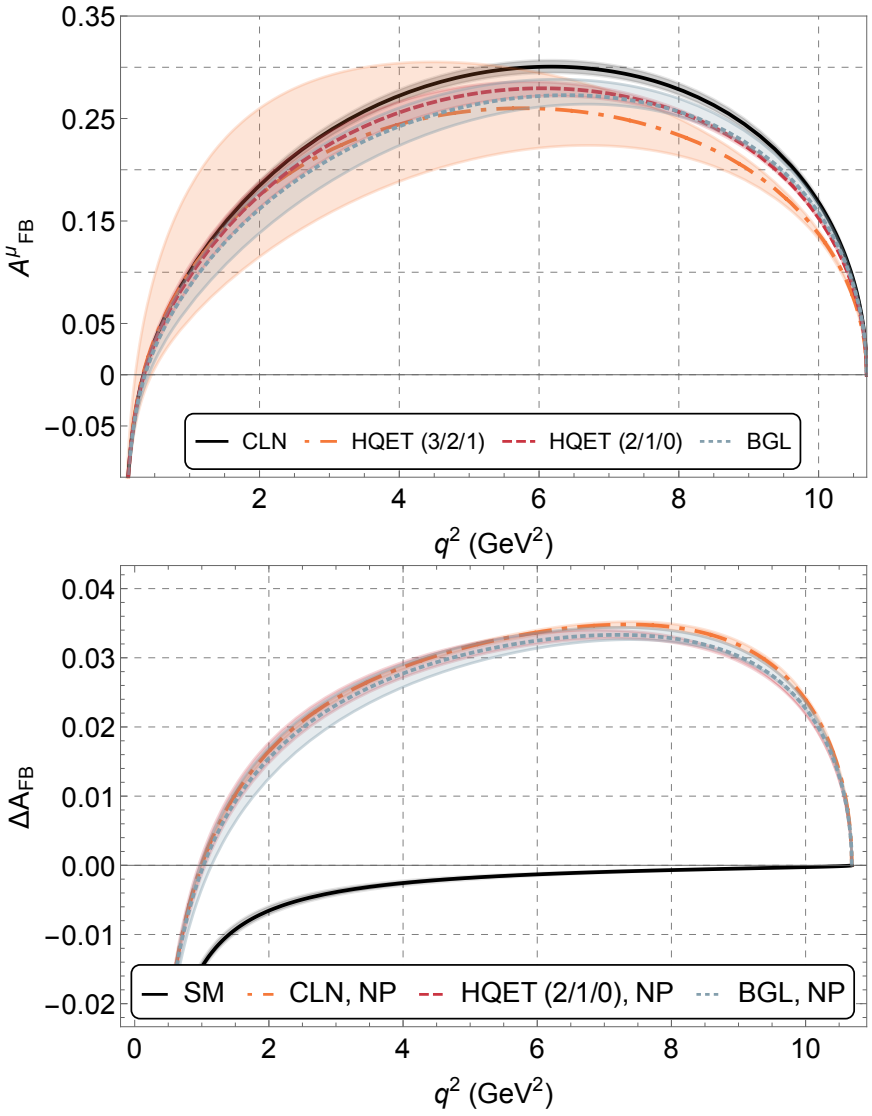

Figure 5.2: A^{μ}_{FB} (top) in the SM and $\Delta A_{FB} = A^{\mu}_{FB} - A^{e}_{FB}$ (bottom) for different form factor parameterizations. The top plot shows the SM predictions for various FF parameterizations, while the bottom plot demonstrates the effects of form factor uncertainties on ΔA_{FB} in NP Scenario 1 ($g_L = 0.06$, $g_R = 0.075$, and $g_P = 0.2i$). The solid black curve in the bottom plot represents the SM prediction for the CLN, HQET, and BGL parameterizations. Note that the vertical scale of the bottom plot is approximately a factor of ten smaller than that of the top plot. Note also the large negative value at the low q^2 limit. A cutoff of 1.14 GeV^2 is chosen to avoid this.

BR constraint we also need to add a g_L NP coupling that is comparable to g_R. In addition, it is also possible to include a g_P contribution, but in order to satisfy the constraints it must be imaginary. We also found that negative or complex values for g_L and g_R are ruled out by these constraints. Fig. 5.3 shows the region of parameter space in the g_L-g_R plane that is excluded by $\frac{\mathcal{B}(B\to D^*\mu\nu)}{\mathcal{B}(B\to D^*e\nu)} = 1.00 \pm 0.03\ (0.06)$ in red and the region in blue excludes $\Delta A_{FB} = 0.0349 \pm 0.0089\ (0.0178)$ when the error is taken in the 68% (95%) C.L. Further, we observe that an additional non-zero imaginary pseudoscalar interaction strength produces an upward shift in the allowed region of g_R while g_L remains almost the same as shown in the right plot of Fig. 5.3. In this section we provide results corresponding to the three distinct NP Scenarios indicated in Table 5.1 chosen with the above constraints.

	g_L	g_R	g_P
Scenario 1:	0.06	0.075	$0.2i$
Scenario 2:	0.08	0.090	$0.6i$
Scenario 3:	0.07	0.075	0

Table 5.1: Values of NP coefficients for three distinct NP scenarios considered in this paper and used for generating the results presented in this section.

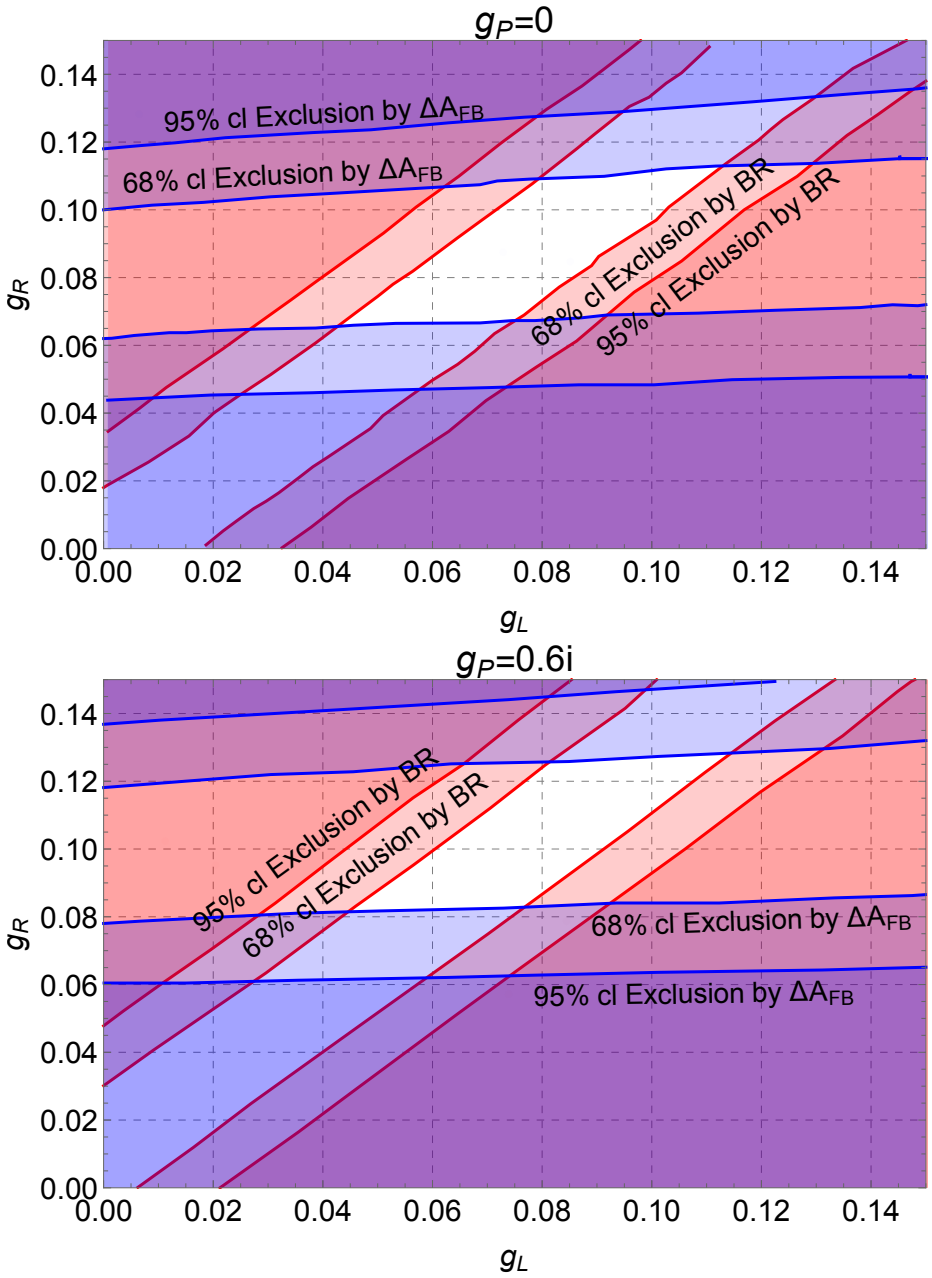

Figure 5.3: Allowed parameter space in g_L and g_R, with $g_P = 0$ and $0.6i$. The two constraints used are that the branching ratio of the muon and electron modes must be unity within 3%, and ΔA_{FB} must be consistent with the value found in Ref. [24]. Non-zero values of g_P produce similar plots, with the allowed region in g_R shifting upwards. This exercise also showed that imaginary values of g_L and g_R are not consistent with these constraints.

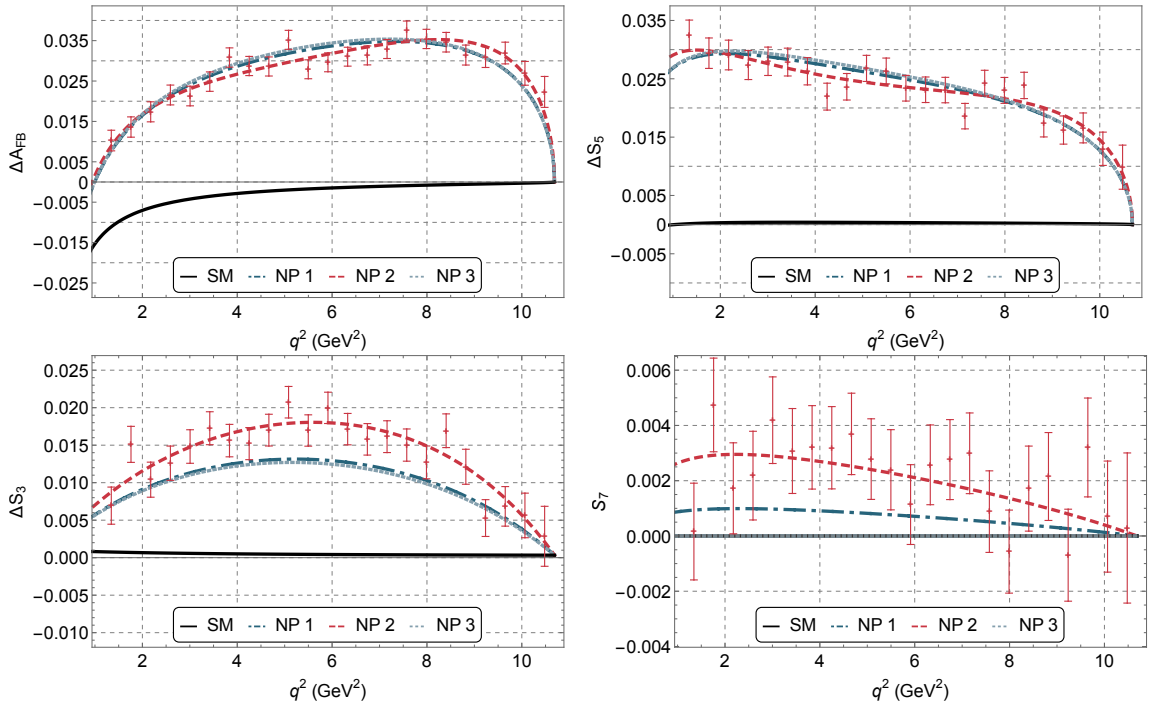

Figure 5.4: ΔA_{FB}, ΔS_5, ΔS_3, and S_7 plotted as functions of q^2 for different values of NP coefficients. Here we have used the CLN parameterizations of the FFs. The NP parameters were chosen so that the ratio of semi-leptonic branching fractions is constrained to be within 3% of unity, as well as the ΔA_{FB} for the full q^2 range is within the interval 0.0349 ± 0.0089. EvtGen data for NP Scenario 2 ($g_L = 0.08$, $g_R = 0.09$, $g_P = 0.6i$) generated with 10^7 events (anticipated Belle II statistics) are shown as points with error bars. Theory curves are presented for all three NP Scenarios: Scenario 1 is dot-dashed blue, Scenario 2 is dashed red and Scenario 3 is dotted blue.

To optimize sensitivity, it is important to measure the Δ observables as functions of q^2. Using the benchmark scenarios above, we show in Fig. 5.4 the predictions for the Δ observables. As discussed earlier these observables are sensitive to NP couplings and have much reduced dependence on form-factor uncertainties. In the figure, the SM expectations for these quantities are shown using solid black curves. In addition to the two Δ observables, ΔA_{FB} and ΔS_5, Fig. 5.4 also shows the q^2 dependence of the observable ΔS_3 and S_7. S_7 represents an angular asymmetry in $\sin\chi$, where χ is the azimuthal angle between the decay planes. This is a CP-odd triple-product asymmetry, which is predicted to be identically zero in the SM for any q^2. We find that NP scenarios with an imaginary g_P are able to produce a small non-zero signal in the q^2 distribution of S_7 as shown in Fig. 5.4.

The observable S_3 is the coefficient of $\cos 2\chi$ term in the angular distribution and can be extracted using the asymmetric integral defined in Eq. (4.2). Although ΔS_3 is close to zero in the SM, NP can produce a non-zero ΔS_3 in the q^2 range as shown in the lower left plot of Fig. 5.4.

Note that due to lepton mass and helicity effects, ΔA_{FB} is negative in the low q^2 region even in the SM. In fact, at the lower momentum transfer threshold, i.e in the limit $q^2 \to m_\ell^2$, the forward-backward asymmetry $A_{FB}^\ell \to -1$ which is seen as a large dip in the q^2 distribution as shown in Fig. 5.2. Hence, for the best experimental sensitivity to NP,

we advocate a necessary low q^2 cut of 1.14 GeV^2 on such observables in order to predict them unambiguosly.

In addition, in order to improve systematic uncertainties from lepton identification efficiencies, we recommend using the same laboratory momentum cutoff for both $\ell = e$ and μ channels (see for example [43]). In order to define the detector acceptance we will represent the magnitude of the transverse momentum of particle x in the lab frame by $|\vec{p}_{T,x}|$ and the ratio of the z-component of the momentum over the total momentum as $\cos\alpha$. We use the Belle II acceptances of $|\vec{p}_{T,\ell}| > 0.8$ GeV for the lepton momenta, $|\vec{p}_{T,\pi}| > 0.1$ GeV for the slow pion momenta, and $-0.866 < \cos\alpha < 0.956$ for all final state particles. The theoretical predictions and uncertainties for these observables integrated over the range of $q^2 \in [1.14\ \text{GeV}^2, (m_B - m_{D^*})^2]$ using the CLN parameterization are displayed in

	$\langle \Delta A_{FB} \rangle$	$\langle \Delta S_3 \rangle$	$\langle \Delta S_5 \rangle$	$\langle S_7 \rangle$
	%	%	%	$\times 10^{-3}$
SM:	-0.252$\pm$0.004	0.0441$\pm$0.0007	0.0286$\pm$0.0013	0
NP 1:	2.89$\pm$0.05	1.08 ± 0.04	$2.44^{+0.02}_{-0.03}$	0.70 ± 0.01
NP 2:	$2.89^{+0.05}_{-0.06}$	$1.49^{+0.05}_{-0.04}$	$2.43^{+0.02}_{-0.03}$	2.0$\pm$0.1
NP 3:	$2.94^{+0.04}_{-0.05}$	1.04$\pm$0.04	$2.47^{+0.03}_{-0.02}$	0

Table 5.2: Theoretical predictions of integrated ΔA_{FB}, ΔS_3, ΔS_5, and S_7 for SM and each NP scenario using the CLN form factor parameterization with estimated theoretical uncertainties. Note that for SM and NP 3, $\langle S_7 \rangle$ is exactly zero as all associated couplings are real.

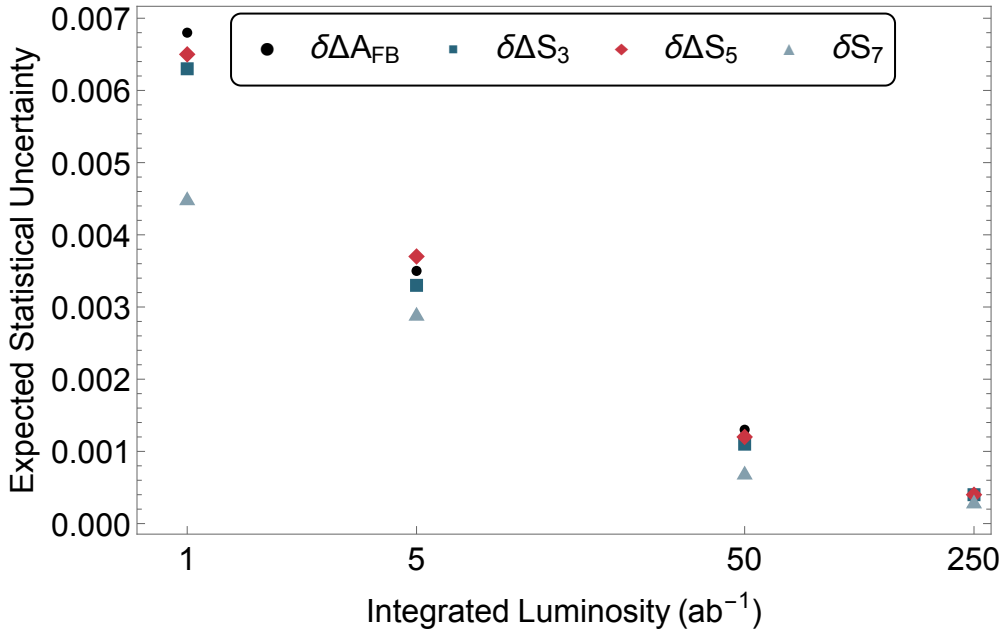

Figure 5.5: Expected statistical uncertainties for the four observables at 1, 5, 50, and 250 ab^{-1} of Belle II data. These expected uncertainties were found using the BTODSTARLNUNP MC simulation.

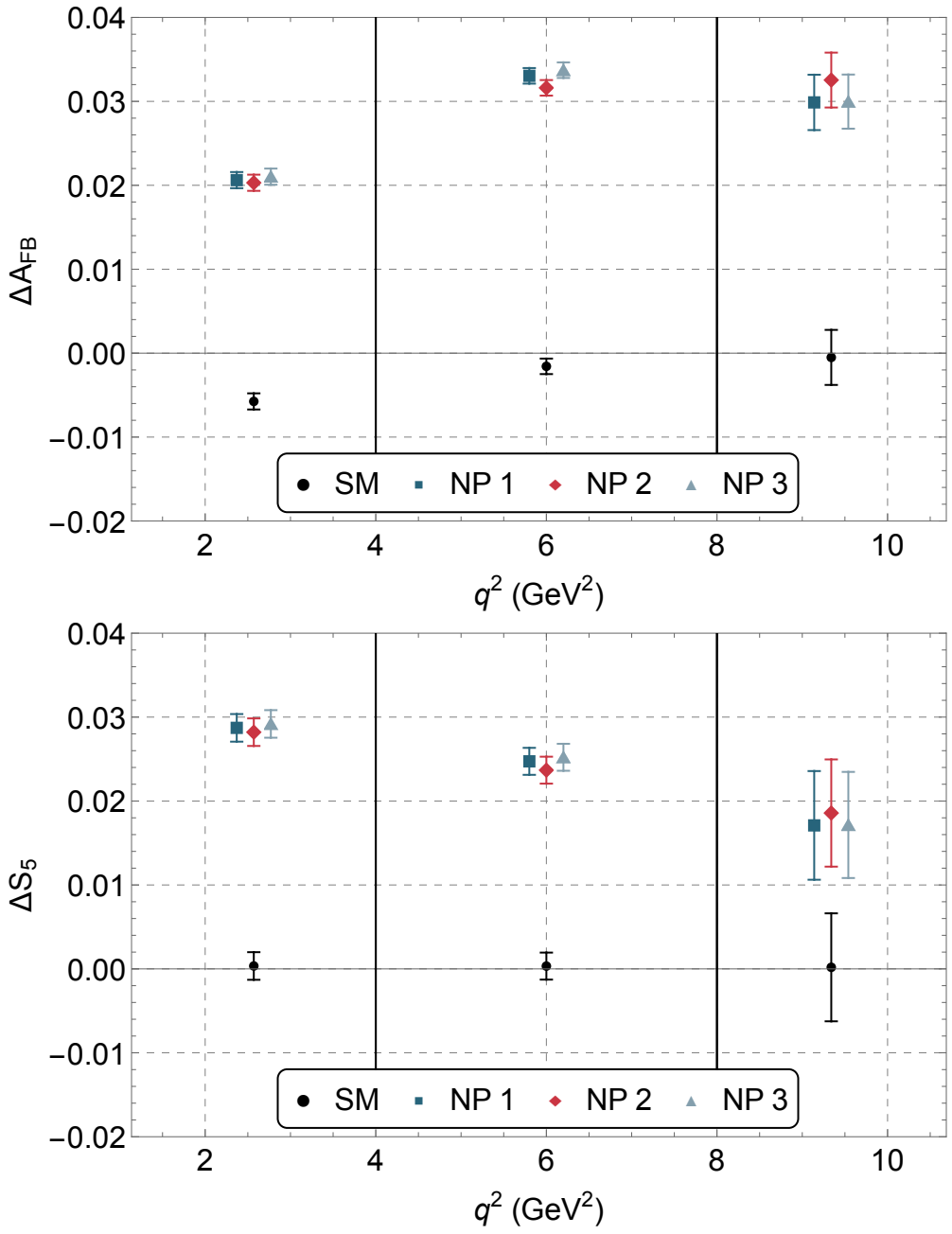

Figure 5.6: Coarse-binned distributions of ΔA_{FB} and ΔS_5 versus q^2. The horizontal axis spans the allowed range for q^2 which has been divided into three bins. The vertical lines at 4 and 8 GeV^2 indicate the other edges of these bins. The central values are calculated from theory, and the error bars indicate statistical uncertainties taken from MC simulation with an integrated luminosity of 50 ab^{-1}. The NP1 and NP3 predictions have been offset from the center of each bin for clarity.

Table. 5.2 both for the SM and the specific NP scenarios listed in Table. 5.1. One can see that the theoretical uncertainties are less than $\sim 5\%$ for both the SM and NP predictions. We also show the variation of the expected statistical uncertainties as a function of the total integrated luminosity for present and future experimental datasets in Fig. 5.5 using MC simulations.

Initially, experiments will measure integrated Δ observables. As statistics improve, they will proceed to coarse-binned measurements, as shown for example, in Fig. 5.6. At high statistics, unbinned fits to angular observables will be performed, as shown for example, in Fig. 5.4.

Furthermore, from Fig. 5.4 we see that NP couplings produce correlated signatures of deviations from the SM in multiple Δ observables, such as ΔA_{FB} and ΔS_5. As shown in Fig. 5.7, the size of the effect on Δ-observables is determined primarily by g_R. In this plot, we have varied the NP parameter g_L between 0 and 0.2 for fixed values of g_R. In the presence of NP there are strong correlations between the Δ-observables ΔA_{FB}, ΔS_5, and ΔS_3. Therefore, if an experimental signal in ΔA_{FB} is observed, it should be accompanied by an observation of non-zero ΔS_5 and ΔS_3. Conversely, if a non-zero ΔS_5 is observed, there must also be a non-zero ΔA_{FB}. In the absence of a tensor coupling, a correlation with ΔS_3 is also required.

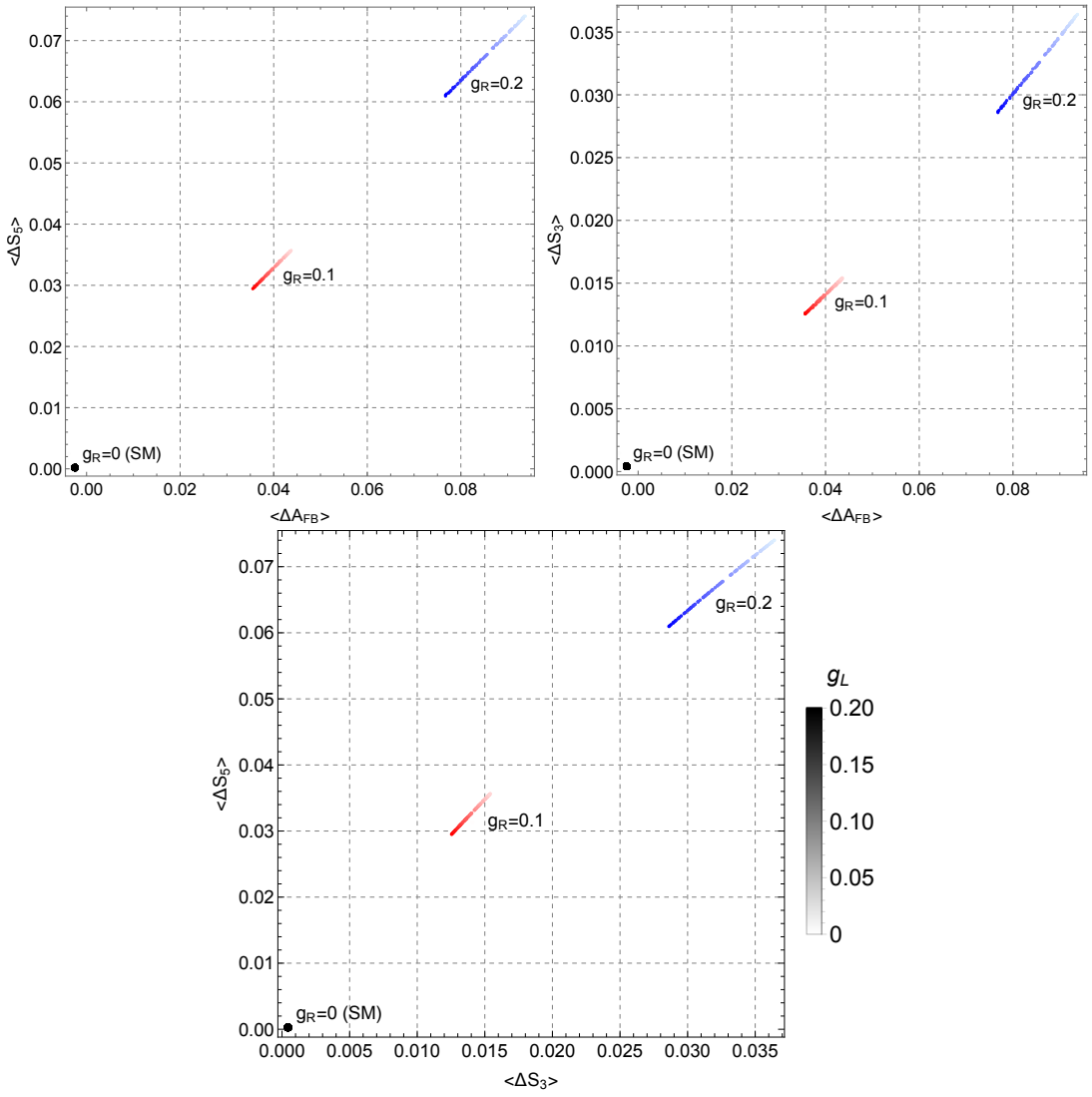

Figure 5.7: Correlations between $\langle \Delta A_{FB} \rangle$, $\langle \Delta S_3 \rangle$, and $\langle \Delta S_5 \rangle$ in NP scenarios. For each point, g_L is varied between 0 and 0.2 (light to dark in the color scale as depicted in the bar legend; applies for each value of g_R), with $g_R = 0$, 0.1, or 0.2, which are representative values in the allowed range, and $g_P = 0$. All points for which only g_L is non-zero return the SM values of the three observables.

For the benchmark scenarios described above, we have also checked the constraints from the longitudinal polarization fraction of the D^* meson, F_L, and another angular observable $\tilde{F}_L$, which are proportional to the coefficients of the $\cos^2\theta^*$ and $\cos^2\theta_\ell$ terms in the angular distribution, respectively. These quantities were extracted for the first time by [24] using the binned CP-averaged differential decay distribution data provided by Belle [10]. They obtain a CP-averaged SM prediction for the integrated $\langle \Delta F_L \rangle$ and $\langle \Delta \tilde{F}_L \rangle$ to be $(5.43 \pm 0.36) \times 10^{-4}$ and $(-5.20 \pm 0.30) \times 10^{-3}$ respectively. By fitting the data, they also report $\langle \Delta F_L \rangle^{exp} = -0.0065 \pm 0.0059$ and $\langle \Delta \tilde{F}_L \rangle^{exp} = -0.0107 \pm 0.0142$. We have verified that our benchmark values satisfy these experimental bounds within a 1σ confidence interval.

CHAPTER 6

CONCLUSIONS

Motivated by the ΔA_{FB} anomaly in $\overline{B} \to D^{*+}\mu^{-}\bar{\nu}$ decay, which could be a sign of physics beyond the Standard Model [24], we have developed a new Monte Carlo New Physics (NP) generator tool for $B \to D^{*}\ell\nu_{\ell}$ with $\ell = e, \mu, \tau$ in the EvtGen framework [37]. The full theoretical description for the effective basis we use to parameterize NP as well as the different angular asymmetries has been comprehensively discussed in this article. We used this tool to examine signatures of NP, which are consistent with current data and with the hints of NP in $B \to D^{*}\mu\nu_{\mu}$ assuming that the decay $B \to D^{*}e\nu_{e}$ is well described by the SM. We found that the angular asymmetries, A_{FB}, S_5, S_3, and S_7, which can be extracted from the fully reconstructed angular distribution, are sensitive to new physics. With current experimental constraints, we show the part of the g_i NP parameter space that is still allowed (see Fig. 5.3).

We introduce the Δ observables, which are obtained by taking the differences between the observables for the muon and the electron modes, in order to avoid theory uncertainties due to form factors, which might obscure signals of NP. We suggest experimental

requirements on q^2 and lepton momenta in order to increase sensitivity to NP and reduce systematics. We identify ΔA_{FB} and ΔS_5 as the most powerful probes of NP with little sensitivity to form-factor uncertainties; this is shown in Fig. 5.2. We also observe that correlated signatures of NP in multiple observables such as ΔA_{FB} and ΔS_5 are required to confirm the presence of NP (see Fig. 5.4.) Therefore, if a NP signal for ΔA_{FB} is observed in future experiments, it must be accompanied by a corresponding signal in ΔS_5 both in the integrated variable and the q^2 distribution. We calculate integrated observables and plot coarse binned expectations for ΔA_{FB} and ΔS_5, as well as correlations between the two. The NP signatures described here are ideally suited for Belle II at 1, 5, 50, and 250 ab^{-1} and might also be explored at hadron collider experiments.

LIST OF REFERENCES

[1] J. P. Lees et al. Evidence for an excess of $\bar{B} \to d^{(*)}\tau^-\bar{\nu}_\tau$ decays. *Phys. Rev. Lett.*, 109:101802 (2012), arXiv:1205.5442 [hep-ex].

[2] J. P. Lees et al. Measurement of an Excess of $\bar{B} \to D^{(*)}\tau^-\bar{\nu}_\tau$ Decays and Implications for Charged Higgs Bosons. *Phys. Rev. D*, 88(7):072012 (2013), arXiv:1303.0571 [hep-ex].

[3] Roel Aaij et al. Measurement of the ratio of branching fractions $\mathcal{B}(\bar{B}^0 \to D^{*+}\tau^-\bar{\nu}_\tau)/\mathcal{B}(\bar{B}^0 \to D^{*+}\mu^-\bar{\nu}_\mu)$. *Phys. Rev. Lett.*, 115(11):111803 (2015), arXiv:1506.08614 [hep-ex]. [Erratum: Phys.Rev.Lett. 115, 159901 (2015)].

[4] M. Huschle et al. Measurement of the branching ratio of $\bar{B} \to D^{(*)}\tau^-\bar{\nu}_\tau$ relative to $\bar{B} \to D^{(*)}\ell^-\bar{\nu}_\ell$ decays with hadronic tagging at Belle. *Phys. Rev. D*, 92(7):072014 (2015), arXiv:1507.03233 [hep-ex].

[5] Y. Sato et al. Measurement of the branching ratio of $\bar{B}^0 \to D^{*+}\tau^-\bar{\nu}_\tau$ relative to $\bar{B}^0 \to D^{*+}\ell^-\bar{\nu}_\ell$ decays with a semileptonic tagging method. *Phys. Rev. D*, 94(7):072007 (2016), arXiv:1607.07923 [hep-ex].

[6] S. Hirose et al. Measurement of the τ lepton polarization and $R(D^*)$ in the decay $\bar{B} \to D^*\tau^-\bar{\nu}_\tau$. *Phys. Rev. Lett.*, 118(21):211801 (2017), arXiv:1612.00529 [hep-ex].

[7] R. Aaij et al. Measurement of the ratio of the $B^0 \to D^{*-}\tau^+\nu_\tau$ and $B^0 \to D^{*-}\mu^+\nu_\mu$ branching fractions using three-prong τ-lepton decays. *Phys. Rev. Lett.*, 120(17):171802 (2018), arXiv:1708.08856 [hep-ex].

[8] S. Hirose et al. Measurement of the τ lepton polarization and $R(D^*)$ in the decay $\bar{B} \to D^*\tau^-\bar{\nu}_\tau$ with one-prong hadronic τ decays at Belle. *Phys. Rev. D*, 97(1):012004 (2018), arXiv:1709.00129 [hep-ex].

[9] R. Aaij et al. Test of Lepton Flavor Universality by the measurement of the $B^0 \to D^{*-}\tau^+\nu_\tau$ branching fraction using three-prong τ decays. *Phys. Rev. D*, 97(7):072013 (2018), arXiv:1711.02505 [hep-ex].

[10] A. Abdesselam et al. Measurement of $\mathcal{R}(D)$ and $\mathcal{R}(D^*)$ with a semileptonic tagging method. Apr 2019, arXiv:1904.08794 [hep-ex].

[11] Yasmine Sara Amhis et al. Averages of b-hadron, c-hadron, and τ-lepton properties as of 2018. *Eur. Phys. J. C*, 81(3):226 (2021), arXiv:1909.12524 [hep-ex].

[12] Ryoutaro Watanabe. New Physics effect on $B_c \to J/\psi\tau\bar{\nu}$ in relation to the $R_{D^{(*)}}$ anomaly. *Phys. Lett. B*, 776:5–9 (2018), arXiv:1709.08644 [hep-ph].

[13] A. Abdesselam et al. Precise determination of the CKM matrix element $|V_{cb}|$ with $\bar{B}^0 \to D^{*+}\,\ell^-\,\bar{\nu}_\ell$ decays with hadronic tagging at Belle. Feb 2017, arXiv:1702.01521 [hep-ex].

[14] Aritra Biswas, Lopamudra Mukherjee, Soumitra Nandi, and Sunando Kumar Patra. Constraining New Physics with Possible Dark Matter Signatures from a Global CKM Fit. Nov 2021, arXiv:2111.01176 [hep-ph].

[15] A. Bazavov et al. Semileptonic form factors for $B \to D^*\ell\nu$ at nonzero recoil from 2 + 1-flavor lattice QCD. May 2021, arXiv:2105.14019 [hep-lat].

[16] E. Waheed et al. Measurement of the CKM matrix element $|V_{cb}|$ from $B^0 \to D^{*-}\ell^+\nu_\ell$ at Belle. *Phys. Rev. D*, 100(5):052007 (2019), arXiv:1809.03290 [hep-ex]. [Erratum: Phys.Rev.D 103, 079901 (2021)].

[17] Bernard Aubert et al. A Measurement of the branching fractions of exclusive $\bar{B} \to D^{(*)}\ (\pi)\ \ell^-\bar{\nu}(\ \ell)$ decays in events with a fully reconstructed B meson. *Phys. Rev. Lett.*, 100:151802 (2008), arXiv:0712.3503 [hep-ex].

[18] B. Abi et al. Measurement of the Positive Muon Anomalous Magnetic Moment to 0.46 ppm. *Phys. Rev. Lett.*, 126(14):141801 (2021), arXiv:2104.03281 [hep-ex].

[19] Roel Aaij et al. Test of lepton universality in beauty-quark decays. *Nature Phys.*, 18(3):277–282 (2022), arXiv:2103.11769 [hep-ex].

[20] Bhubanjyoti Bhattacharya, Alakabha Datta, David London, and Shanmuka Shivashankara. Simultaneous Explanation of the R_K and $R(D^{(*)})$ Puzzles. *Phys. Lett. B*, 742:370–374 (2015), arXiv:1412.7164 [hep-ph].

[21] Bhubanjyoti Bhattacharya, Alakabha Datta, Saeed Kamali, and David London. CP Violation in $\bar{B}^0 \to D^{*+}\mu^-\bar{\nu}_\mu$. *JHEP*, 05:191 (2019), arXiv:1903.02567 [hep-ph].

[22] Murugeswaran Duraisamy and Alakabha Datta. The Full $B \to D^*\tau^-\bar{\nu_\tau}$ Angular Distribution and CP violating Triple Products. *JHEP*, 09:059 (2013), arXiv:1302.7031 [hep-ph].

[23] Murugeswaran Duraisamy, Preet Sharma, and Alakabha Datta. Azimuthal $B \to D^* \tau^- \bar{\nu_\tau}$ angular distribution with tensor operators. *Phys. Rev. D*, 90(7):074013 (2014), arXiv:1405.3719 [hep-ph].

[24] Christoph Bobeth, Marzia Bordone, Nico Gubernari, Martin Jung, and Danny van Dyk. Lepton-flavour non-universality of $\bar{B} \to D^* \ell \bar{\nu}$ angular distributions in and beyond the Standard Model. *Eur. Phys. J. C*, 81(11):984 (2021), arXiv:2104.02094 [hep-ph].

[25] Alexandre Carvunis, Andreas Crivellin, Diego Guadagnoli, and Shireen Gangal. The Forward-Backward Asymmetry in $B \to D^* \ell \nu$: One more hint for Scalar Leptoquarks? *Phys. Rev. D*, 105(3):L031701 (2022), arXiv:2106.09610 [hep-ph].

[26] Alakabha Datta, Hongkai Liu, and Danny Marfatia. $\bar{B} \to D^{(*)} \ell \bar{X}$ decays in effective field theory with massive right-handed neutrinos. Apr 2022, arXiv:2204.01818 [hep-ph].

[27] Bhubanjyoti Bhattacharya, Alakabha Datta, Saeed Kamali, and David London. A measurable angular distribution for $\overline{B} \to D^* \tau^- \overline{v}_\tau$ decays. *JHEP*, 07(07):194 (2020), arXiv:2005.03032 [hep-ph].

[28] Yasuhito Sakaki, Minoru Tanaka, Andrey Tayduganov, and Ryoutaro Watanabe. Testing leptoquark models in $\bar{B} \to D^{(*)} \tau \bar{\nu}$. *Phys. Rev. D*, 88(9):094012 (2013), arXiv:1309.0301 [hep-ph].

[29] Michael E. Peskin and Daniel V. Schroeder. *An Introduction to quantum field theory*. Addison-Wesley, Reading, USA, 1995.

[30] Michael E. Peskin. Corrections to An Introduction to quantum field theory.

[31] James Gratrex, Markus Hopfer, and Roman Zwicky. Generalised helicity formalism, higher moments and the $B \to K_{J_K} (\to K\pi) \bar{\ell}_1 \ell_2$ angular distributions. *Phys. Rev. D*, 93(5):054008 (2016), arXiv:1506.03970 [hep-ph].

[32] Wolfgang Altmannshofer, Patricia Ball, Aoife Bharucha, Andrzej J. Buras, David M. Straub, and Michael Wick. Symmetries and Asymmetries of $B \to K^* \mu^+ \mu^-$ Decays in the Standard Model and Beyond. *JHEP*, 01:019 (2009), arXiv:0811.1214 [hep-ph].

[33] Christoph Bobeth, Gudrun Hiller, and Giorgi Piranishvili. CP Asymmetries in bar $B \to \bar{K}^*(\to \bar{K}\pi)\bar{\ell}\ell$ and Untagged $\bar{B}_s$, $B_s \to \phi(\to K^+K^-)\bar{\ell}\ell$ Decays at NLO. *JHEP*, 07:106 (2008), arXiv:0805.2525 [hep-ph].

[34] Alakabha Datta and David London. Triple-product correlations in B –> V1 V2 decays and new physics. *Int. J. Mod. Phys. A*, 19:2505–2544 (2004), arXiv:hep-ph/0303159.

[35] Michael Gronau and Jonathan L. Rosner. Triple product asymmetries in K, $D_{(s)}$ and $B_{(s)}$ decays. *Phys. Rev. D*, 84:096013 (2011), arXiv:1107.1232 [hep-ph].

[36] D. J. Lange. The EvtGen particle decay simulation package. *Nucl. Instrum. Meth. A*, 462:152, 2001.

[37] Q. Campagna et al. A new tool to search for physics beyond the Standard Model in $\bar{B} \to D^{*+}\ell^-\bar{\nu}$.

[38] Irinel Caprini, Laurent Lellouch, and Matthias Neubert. Dispersive bounds on the shape of $\bar{B} \to D^{(*)}\ell\bar{\nu}$ form-factors. *Nucl. Phys. B*, 530:153–181 (1998), arXiv:hep-ph/9712417.

[39] C. Glenn Boyd, Benjamin Grinstein, and Richard F. Lebed. Precision corrections to dispersive bounds on form-factors. *Phys. Rev. D*, 56:6895–6911 (1997), arXiv:hep-ph/9705252.

[40] Marzia Bordone, Martin Jung, and Danny van Dyk. Theory determination of $\bar{B} \to D^{(*)}\ell^-\bar{\nu}$ form factors at $\mathcal{O}(1/m_c^2)$. *Eur. Phys. J. C*, 80(2):74 (2020), arXiv:1908.09398.

[41] R. N. Faustov, V. O. Galkin, and Xian-Wei Kang. Relativistic description of the semileptonic decays of bottom mesons. *Phys. Rev. D*, 106(1):013004 (2022), arXiv:2206.10277 [hep-ph].

[42] Florian U. Bernlochner, Zoltan Ligeti, Michele Papucci, Markus T. Prim, Dean J. Robinson, and Chenglu Xiong. Constrained second-order power corrections in HQET: $R(D^{(*)})$, $|V_{cb}|$, and new physics. June 2022, arXiv:2206.11281 [hep-ph].

[43] Florian Herren. The forward-backward asymmetry and differences of partial moments in inclusive semileptonic B decays. May 2022, arXiv:2205.03427 [hep-ph].

[44] M. Beneke and T. Feldmann. Symmetry breaking corrections to heavy to light B meson form-factors at large recoil. *Nucl. Phys. B*, 592:3–34 (2001), arXiv:hep-ph/0008255.

[45] P.A. Zyla et al. Review of Particle Physics. *PTEP*, 2020(8):083C01, 2020.

[46] Nathan Isgur and Mark B. Wise. Excited charm mesons in semileptonic anti-B decay and their contributions to a Bjorken sum rule. *Phys. Rev. D*, 43:819–828, 1991.

[47] Matthias Neubert. Heavy quark symmetry. *Phys. Rept.*, 245:259–396 (1994), arXiv:hep-ph/9306320.

[48] Syuhei Iguro and Ryoutaro Watanabe. Bayesian fit analysis to full distribution data of $\overline{\mathrm{B}} \to \mathrm{D}^{(*)}\ell\overline{\nu} : |\mathrm{V_{cb}}|$ determination and new physics constraints. *JHEP*, 08(08):006 (2020), arXiv:2004.10208 [hep-ph].

[49] Adam F. Falk and Matthias Neubert. Second order power corrections in the heavy quark effective theory. 1. Formalism and meson form-factors. *Phys. Rev. D*, 47:2965–2981 (1993), arXiv:hep-ph/9209268.

[50] Dante Bigi, Paolo Gambino, and Stefan Schacht. $R(D^*)$, $|V_{cb}|$, and the Heavy Quark Symmetry relations between form factors. *JHEP*, 11:061 (2017), arXiv:1707.09509 [hep-ph].

[51] P. Gambino et al. Challenges in semileptonic B decays. *Eur. Phys. J. C*, 80(10):966 (2020), arXiv:2006.07287 [hep-ph].

LIST OF APPENDICES

APPENDIX A

ANGULAR COEFFICIENTS

The angular distribution of $\overline{B} \to D^* \ell^- \bar{\nu}$ presented in Eq. (2.11) contains 12 coefficients labeled $I_i^{(s,c)}$ with $i = 1, \ldots, 9$. The full list of angular coefficients are presented below as functions of eight helicity amplitudes, $\mathcal{A}_{SP}, \mathcal{A}_t, \mathcal{A}_0, \mathcal{A}_{||}, \mathcal{A}_\perp, \mathcal{A}_{0T}, \mathcal{A}_{||,T}$, and $\mathcal{A}_{\perp,T}$. These helicity amplitudes depend on hadronic form factors as well as NP coefficients. The form of the eight helicity amplitudes are given in Appendix B.

$$I_i^{(s,c)} = \frac{G_F^2 |V_{cb}|^2 (q^2 - m_\ell^2)^2 |p_{D^*}|}{192\pi^3 m_B^2 q^2} \mathcal{B}(D^* \to D\pi) \tilde{I}_i^{(s,c)}, \tag{A.1}$$

$$\begin{aligned}\tilde{I}_1^c = {} & 4\left(|\mathcal{A}_{SP}|^2 + \frac{m_\ell^2}{q^2}|\mathcal{A}_t|^2\right) + 2\left(1 + \frac{m_\ell^2}{q^2}\right)\left(|\mathcal{A}_0|^2 + 16\,|\mathcal{A}_{0,T}|^2\right) \\ & + 8\,\frac{m_\ell}{\sqrt{q^2}}\left\{\mathrm{Re}\left[\mathcal{A}_t \mathcal{A}_{SP}^*\right] - 4\,\mathrm{Re}\left[\mathcal{A}_0 \mathcal{A}_{0,T}^*\right]\right\},\end{aligned} \tag{A.2}$$

$$\begin{aligned}\tilde{I}_1^s = {} & \left\{\frac{3}{2}(|\mathcal{A}_{||}|^2 + |\mathcal{A}_\perp|^2) + 8(|\mathcal{A}_{||,T}|^2 + |\mathcal{A}_{\perp,T}|^2)\right\} \\ & - 16\,\frac{m_\ell}{\sqrt{q^2}}\left\{\mathrm{Re}[\mathcal{A}_{||}\mathcal{A}_{||,T}^*] + \mathrm{Re}[\mathcal{A}_\perp \mathcal{A}_{\perp,T}^*]\right\} \\ & + \frac{m_\ell^2}{q^2}\left\{\frac{1}{2}\left(|\mathcal{A}_{||}|^2 + |\mathcal{A}_\perp|^2\right) + 24\left(|\mathcal{A}_{||,T}|^2 + |\mathcal{A}_{\perp,T}|^2\right)\right\},\end{aligned} \tag{A.3}$$

$$\tilde{I}_2^c = -2\left(1 - \frac{m_\ell^2}{q^2}\right)\left\{|\mathcal{A}_0|^2 - 16|\mathcal{A}_{0,T}|^2\right\}, \tag{A.4}$$

$$\tilde{I}_2^s = \frac{1}{2}\left(1 - \frac{m_\ell^2}{q^2}\right)\left\{\left(|\mathcal{A}_{||}|^2 + |\mathcal{A}_\perp|^2\right) - 16\left(|\mathcal{A}_{||,T}|^2 + |\mathcal{A}_{\perp,T}|^2\right)\right\}, \tag{A.5}$$

$$\tilde{I}_3 = -\left(1 - \frac{m_\ell^2}{q^2}\right)\left\{\left(|\mathcal{A}_{||}|^2 - |\mathcal{A}_\perp|^2\right) - 16\left(|\mathcal{A}_{||,T}|^2 - |\mathcal{A}_{\perp,T}|^2\right)\right\}, \tag{A.6}$$

$$\tilde{I}_4 = \sqrt{2}\left(1 - \frac{m_\ell^2}{q^2}\right)\left\{16\,\mathrm{Re}\left[\mathcal{A}_{0,T}\mathcal{A}_{||,T}^*\right] - \mathrm{Re}\left[\mathcal{A}_0 \mathcal{A}_{||}^*\right]\right\}, \tag{A.7}$$

$$\tilde{I}_5 = 2\sqrt{2}\left\{\left(\mathrm{Re}\left[\mathcal{A}_0 \mathcal{A}_\perp^*\right] + 4\,\mathrm{Re}\left[\mathcal{A}_{||,T}\mathcal{A}_{SP}^*\right]\right) + \frac{m_\ell^2}{q^2}\left(16\,\mathrm{Re}\left[\mathcal{A}_{0,T}\mathcal{A}_{\perp,T}^*\right] - \mathrm{Re}\left[\mathcal{A}_{||}\mathcal{A}_t^*\right]\right)\right.$$

$$+ \frac{m_\ell}{\sqrt{q^2}} \left(4\,\mathrm{Re}\left[\mathcal{A}_{||,T}\mathcal{A}_t^*\right] - 4\,\mathrm{Re}\left[\mathcal{A}_0\mathcal{A}_{\perp,T}^*\right] - 4\,\mathrm{Re}\left[\mathcal{A}_{0,T}\mathcal{A}_\perp^*\right] - \mathrm{Re}\left[\mathcal{A}_{||}\mathcal{A}_{SP}^*\right] \right) \Bigg\}, \tag{A.8}$$

$$\tilde{I}_6^c = 32\,\mathrm{Re}\left[\mathcal{A}_{0,T}\mathcal{A}_{SP}^*\right] + \frac{m_\ell}{\sqrt{q^2}} \left\{ 32\,\mathrm{Re}\left[\mathcal{A}_{0,T}\mathcal{A}_t^*\right] - 8\mathrm{Re}\left[\mathcal{A}_0\mathcal{A}_{SP}^*\right] \right\} - 8\,\frac{m_\ell^2}{q^2}\mathrm{Re}\left[\mathcal{A}_0\mathcal{A}_t^*\right], \tag{A.9}$$

$$\begin{aligned} \tilde{I}_6^s = &- 4\,\mathrm{Re}\left[\mathcal{A}_{||}\mathcal{A}_\perp^*\right] + 16\,\frac{m_\ell}{\sqrt{q^2}} \left\{ \mathrm{Re}\left[\mathcal{A}_{||}\mathcal{A}_{\perp,T}^*\right] + \mathrm{Re}\left[\mathcal{A}_{||,T}\mathcal{A}_\perp^*\right] \right\} \\ &- 64\,\frac{m_\ell^2}{q^2}\,\mathrm{Re}\left[\mathcal{A}_{||,T}\mathcal{A}_{\perp,T}^*\right], \end{aligned} \tag{A.10}$$

$$\begin{aligned} \tilde{I}_7 = &- 8\sqrt{2}\,\mathrm{Im}\left[\mathcal{A}_{SP}\mathcal{A}_{\perp,T}^*\right] - 2\sqrt{2}\,\mathrm{Im}\left[\mathcal{A}_0\mathcal{A}_{||}^*\right] + 2\sqrt{2}\,\frac{m_\ell^2}{q^2}\,\mathrm{Im}\left[\mathcal{A}_t\mathcal{A}_\perp^*\right] \\ &+ 2\sqrt{2}\,\frac{m_\ell}{\sqrt{q^2}} \left\{ 4\,\mathrm{Im}\left[\mathcal{A}_0\mathcal{A}_{||,T}^*\right] - 4\,\mathrm{Im}\left[\mathcal{A}_{||}\mathcal{A}_{0,T}^*\right] - 4\,\mathrm{Im}\left[\mathcal{A}_t\mathcal{A}_{\perp,T}^*\right] - \mathrm{Im}\left[\mathcal{A}_\perp\mathcal{A}_{SP}^*\right] \right\}, \end{aligned} \tag{A.11}$$

$$\tilde{I}_8 = -\sqrt{2}\,\left(1 - \frac{m_\ell^2}{q^2}\right) \mathrm{Im}\left[\mathcal{A}_\perp\mathcal{A}_0^*\right], \tag{A.12}$$

$$\tilde{I}_9 = 2\,\left(1 - \frac{m_\ell^2}{q^2}\right) \mathrm{Im}\left[\mathcal{A}_{||}\mathcal{A}_\perp^*\right], \tag{A.13}$$

where $|p_{D^*}| = \sqrt{\lambda(m_B^2, m_{D^*}^2, q^2)}/(2m_B)$ represents the magnitude of the D^* 3-momentum, and $\lambda(a,b,c) = a^2 + b^2 + c^2 - 2ab - 2bc - 2ca$.

APPENDIX B

HELICITY AMPLITUDES AND FORM FACTORS

The 12 angular coefficients needed to construct the full angular distribution of Eq. (2.11) were presented in Appendix A. These angular coefficients depend on eight helicity amplitudes that can be further expressed in terms of NP coefficients (g_P, g_L, g_R, and g_T) and hadronic form factors. We list the helicity amplitudes below [28, 44].

$$\mathcal{A}_{SP} = -g_P \frac{\sqrt{\lambda(m_B^2, m_{D^*}^2, q^2)}}{m_b + m_c} A_0(q^2), \tag{B.1}$$

$$\mathcal{A}_0 = -\frac{(1 + g_L - g_R)(m_B + m_{D^*})}{2m_{D^*}\sqrt{q^2}} \big[(m_B^2 - m_{D^*}^2 - q^2) A_1(q^2) - \frac{\lambda(m_B^2, m_{D^*}^2, q^2)}{(m_B + m_{D^*})^2} A_2(q^2)\big], \tag{B.2}$$

$$\mathcal{A}_t = -(1 + g_L - g_R) \frac{\sqrt{\lambda(m_B^2, m_{D^*}^2, q^2)}}{\sqrt{q^2}} A_0(q^2), \tag{B.3}$$

$$\mathcal{A}_\pm = (1 + g_L - g_R)\,(m_B + m_{D^*}) A_1(q^2) \mp (1 + g_L + g_R) \frac{\sqrt{\lambda(m_B^2, m_{D^*}^2, q^2)}}{m_B + m_{D^*}} V(q^2), \tag{B.4}$$

$$\mathcal{A}_{0,T} = \frac{g_T}{2m_{D^*}(m_B^2 - m_{D^*}^2)} \big[(m_B^2 - m_{D^*}^2)(m_B^2 + 3m_{D^*}^2 - q^2) T_2(q^2) - \lambda(m_B^2, m_{D^*}^2, q^2) T_3(q^2)\big], \tag{B.5}$$

$$\mathcal{A}_{\pm,T} = g_T \frac{\sqrt{\lambda(m_B^2, m_{D^*}^2, q^2)} T_1(q^2) \pm (m_B^2 - m_{D^*}^2) T_2(q^2)}{\sqrt{q^2}}. \tag{B.6}$$

The angular coefficients requiring vector and/or tensor type contributions may also require the amplitudes to be expressed in the transversity basis as follows.

$$\mathcal{A}_{||,T} = \left(\mathcal{A}_{+(,T)} + \mathcal{A}_{-(,T)}\right)/\sqrt{2}, \tag{B.7}$$

$$\mathcal{A}_{\perp,T} = \left(\mathcal{A}_{+(,T)} - \mathcal{A}_{-(,T)}\right)/\sqrt{2}. \tag{B.8}$$

The above helicity amplitudes depend on the seven hadronic form factors listed below.

$$V(q^2) = \frac{m_B + m_{D^*}}{2\sqrt{m_B m_{D^*}}} h_V(w(q^2)), \tag{B.9}$$

$$A_1(q^2) = \frac{(m_B + m_{D^*})^2 - q^2}{2\sqrt{m_B m_{D^*}}(m_B + m_{D^*})} h_{A_1}(w(q^2)), \tag{B.10}$$

$$A_2(q^2) = \frac{m_B + m_{D^*}}{2\sqrt{m_B m_{D^*}}} \left[h_{A_3}(w(q^2)) + \frac{m_{D^*}}{m_B} h_{A_2}(w(q^2)) \right], \tag{B.11}$$

$$\begin{aligned} A_0(q^2) = \frac{1}{2\sqrt{m_B m_{D^*}}} \Bigg[& \frac{(m_B + m_{D^*})^2 - q^2}{2m_{D^*}} h_{A_1}(w(q^2)) \\ & - \frac{m_B^2 - m_{D^*}^2 + q^2}{2m_B} h_{A_2}(w(q^2)) - \frac{m_B^2 - m_{D^*}^2 - q^2}{2m_{D^*}} h_{A_3}(w(q^2)) \Bigg], \end{aligned} \tag{B.12}$$

$$T_1(q^2) = \frac{1}{2\sqrt{m_B m_{D^*}}} \left[(m_B + m_{D^*}) h_{T_1}(w(q^2)) - (m_B - m_{D^*}) h_{T_2}(w(q^2)) \right], \tag{B.13}$$

$$\begin{aligned} T_2(q^2) = \frac{1}{2\sqrt{m_B m_{D^*}}} \Bigg[& \frac{(m_B + m_{D^*})^2 - q^2}{m_B + m_{D^*}} h_{T_1}(w(q^2)) \\ & - \frac{(m_B - m_{D^*})^2 - q^2}{m_B - m_{D^*}} h_{T_2}(w(q^2)) \Bigg], \end{aligned} \tag{B.14}$$

$$\begin{aligned} T_3(q^2) = \frac{1}{2\sqrt{m_B m_{D^*}}} \Big[& (m_B - m_{D^*}) h_{T_1}(w(q^2)) - (m_B + m_{D^*}) h_{T_2}(w(q^2)) \\ & - 2\frac{m_B^2 - m_{D^*}^2}{m_B} h_{T_3}(w(q^2)) \Bigg], \end{aligned} \tag{B.15}$$

where the recoil angle, $w(q^2)$ can be expressed as is $w(q^2) = (m_B^2 + m_{D^*}^2 - q^2)/2m_B m_{D^*}$. The above expressions depend on several lepton and meson masses that are used as input parameters. In our calculations we use the values of meson and lepton masses given in Table B.1. We have also used the following values for the quark masses, $m_b = 4.18$ GeV and $m_c = 2.54$ GeV.

Masses	Value (MeV)
m_{B^0}	$5279.63(20)$
$m_{D^{*+}}$	$2010.26(05)$
m_e	$0.5109989461(31)$
m_μ	$105.6583745(24)$

Table B.1: Input values used for meson and lepton masses taken from the Particle Data Group [45]. Numbers in parentheses represent the errors in the last two digits.

Note that the above form factors still depend on several additional functions of q^2, namely h_V, h_{A_1}, h_{A_2}, h_{A_3}, h_{T_1}, h_{T_2}, h_{T_3}, R_1, R_2, and R_3. There are several ways of parameterizing these functions using Heavy Quark Effective Theory (HQET). Two such parameterizations are presented in Appendix C.

APPENDIX C

PARAMETERIZATIONS OF THE HADRONIC FORM FACTORS

The hadronic form factors described in Appendix B depend on several form factors that appear as functions of q^2 in HQET. At present there are several ways of parameterizing these functions. Although each parameterization gives a slightly different value for the underlying function, a conclusive identification of the best way to parameterize these functions still eludes us. This problem adds to the theoretical uncertainties associated with the determinations of some of the NP observables discussed in this article.

A commonly used parameterization for the HQET form factors, first presented by Caprini, Lellouch, and Neubert (CLN) in Ref. [38] is given below.

$$h_V(w) = R_1(w) h_{A_1}(w), \tag{C.1}$$

$$h_{A_2}(w) = \frac{R_2(w) - R_3(w)}{2 r_{D^*}} h_{A_1}(w), \tag{C.2}$$

$$h_{A_3}(w) = \frac{R_2(w) + R_3(w)}{2} h_{A_1}(w), \tag{C.3}$$

$$h_{T_1}(w) = \frac{1}{2(1 + r_{D^*}^2 - 2 r_{D^*} w)} \left[\frac{m_b - m_c}{m_B - m_{D^*}} (1 - r_{D^*})^2 (w+1)\, h_{A_1}(w) - \frac{m_b + m_c}{m_B + m_{D^*}} (1 + r_{D^*})^2 (w-1)\, h_V(w) \right], \tag{C.4}$$

$$h_{T_2}(w) = \frac{(1 - r_{D^*}^2)(w+1)}{2(1 + r_{D^*}^2 - 2 r_{D^*} w)} \left[\frac{m_b - m_c}{m_B - m_{D^*}}\, h_{A_1}(w) - \frac{m_b + m_c}{m_B + m_{D^*}}\, h_V(w) \right], \tag{C.5}$$

$$\begin{aligned} h_{T_3}(w) = -\frac{1}{2(1 + r_{D^*})(1 + r_{D^*}^2 - 2 r_{D^*} w)} \Bigg[& 2 \frac{m_b - m_c}{m_B - m_{D^*}} r_{D^*} (w+1)\, h_{A_1}(w) \\ & + \frac{m_b - m_c}{m_B - m_{D^*}} (1 + r_{D^*}^2 - 2 r_{D^*} w)(h_{A_3}(w) - r_{D^*} h_{A_2}(w)) \\ & - \frac{m_b + m_c}{m_B + m_{D^*}} (1 + r_{D^*})^2\, h_V(w) \Bigg], \end{aligned} \tag{C.6}$$

where $r_{D^*} = m_{D^*}/m_B$ and the w-dependencies are expressed as

$$h_{A_1}(w) = h_{A_1}(1)\left[1 - 8\rho^2_{D^*}z + (53\rho^2_{D^*} - 15)z^2 - (231\rho^2_{D^*} - 91)z^3\right] \quad \text{(C.7)}$$

$$R_1(w) = R_1(1) - 0.12(w-1) + 0.05(w-1)^2, \quad \text{(C.8)}$$

$$R_2(w) = R_2(1) + 0.11(w-1) - 0.06(w-1)^2, \quad \text{(C.9)}$$

$$R_3(w) = 1.22 - 0.052(w-1) + 0.026(w-1)^2. \quad \text{(C.10)}$$

The parameter z is related to the recoil angle w through $z(w) = (\sqrt{w+1}-\sqrt{2})/(\sqrt{w+1}+\sqrt{2})$.

Parameter	Value
$h_{A_1}(1)$	0.908 ± 0.017
$\rho^2_{D^*}$	1.207 ± 0.026
$R_1(1)$	1.403 ± 0.033
$R_2(1)$	0.854 ± 0.020

Table C.1: Input values of parameters needed for the CLN parameterization of form factors used here were taken from [28].

Yet another way of parameterizing the HQET form factors is to express them in terms of the leading Isgur-Wise (IW) function $\xi(w)$ [46] and sub-leading IW terms, which represents higher order power corrections to the leading IW function as

$$h_X(w) = \xi(w)\hat{h}_X(w), \quad (X = V, A_1, A_2, A_3, T_1, T_2, T_3) \quad \text{(C.11)}$$

where

$$\hat{h}_X(w) = \hat{h}_{X,0} + \varepsilon_a\, \delta\hat{h}_{X,\alpha_s} + \varepsilon_b\, \delta\hat{h}_{X,m_b} + \varepsilon_c\, \delta\hat{h}_{X,m_c} + \varepsilon_c^2\, \delta\hat{h}_{X,m_c^2}. \tag{C.12}$$

Here, $\varepsilon_a, \varepsilon_b, \varepsilon_c$ denote the expansion coefficients corresponding to the higher order corrections in α_s and $1/m_{b,c}$ respectively which were worked out by [38, 47] using heavy quark symmetry.

The leading term in C.12 is

$$\hat{h}_{X,0} = \begin{cases} 1 \;\text{ for }\; \mathrm{X} = \mathrm{A}_1, \mathrm{A}_3, \mathrm{T}_1, \\ \\ 0 \;\text{ for }\; \mathrm{X} = \mathrm{A}_2, \mathrm{T}_2, \mathrm{T}_3. \end{cases} \tag{C.13}$$

The α_s corrections are given as

$$\delta\hat{h}_{V,\alpha_s} = \frac{1}{6z_{cb}(w-w_{cb})}\left[4z_{cb}(w-w_{cb})\Omega_w(w) + 2(w+1)((3w-1)z_{cb} - z_{cb}^2 - 1)r_w(w)\right.$$
$$\left. -12z_{cb}(w-w_{cb}) - (z_{cb}^2-1)\log z_{cb}\right] + V(\mu)\,, \tag{C.14}$$

$$\delta\hat{h}_{A_1,\alpha_s} = \frac{1}{6z_{cb}(w-w_{cb})}\left[4z_{cb}(w-w_{cb})\Omega_w(w) + 2(w-1)((3w+1)z_{cb} - z_{cb}^2 - 1)r_w(w)\right.$$
$$\left. -12z_{cb}(w-w_{cb}) - (z_{cb}^2-1)\log z_{cb}\right] + V(\mu)\,, \tag{C.15}$$

$$\delta\hat{h}_{A_2,\alpha_s} = \frac{-1}{6z_{cb}^2(w-w_{cb})^2}\left[\left(2 + (2w^2-5w-1)z_{cb} + 2w(2w-1)z_{cb}^2\right.\right.$$
$$\left. +(1-w)z_{cb}^3\right) r_w(w) - 2z_{cb}(z_{cb}+1)(w-w_{cb})$$
$$\left. +(z_{cb}^2 - (4w+2)z_{cb} + 3 + 2w)z_{cb}\log z_{cb}\right]\,, \tag{C.16}$$

$$\delta\hat{h}_{A_3,\alpha_s} = \delta\hat{h}_{A_1,\alpha_s} + \frac{1}{6z_{cb}(w-w_{cb})^2}\left[2z_{cb}(z_{cb}+1)(w_{cb}-w)\right.$$

$$+\big(2z_{cb}^3+z_{cb}^2(2w^2-5w-1)+z_{cb}(4w^2-2w)-w+1\big)r_w(w)$$

$$-\big(z_{cb}^2(2w+3)\,-z_{cb}(4w+2)+1\big)\log z_{cb}\Big] \tag{C.17}$$

$$\delta\hat{h}_{T_1,\alpha_s}=\frac{1}{3z_{cb}(w-w_{cb})}\Big[2z_{cb}(w-w_{cb})\Omega_w(w)+2z_{cb}(w^2-1)r_w(w)-6z_{cb}(w-w_{cb})$$

$$+(1-z_{cb}^2)\log z_{cb}\Big]+T(\mu)\,, \tag{C.18}$$

$$\delta\hat{h}_{T_2,\alpha_s}=\frac{w+1}{3z_{cb}(w-w_{cb})}\left[(1-z_{cb}^2)r_w(w)+2z_{cb}\log z_{cb}\right]\,, \tag{C.19}$$

$$\delta\hat{h}_{T_3,\alpha_s}=\frac{1}{3z_{cb}(w-w_{cb})}\left[(z_{cb}w-1)r_w(w)-z_{cb}\log z_{cb}\right]\,, \tag{C.20}$$

where

$$z_{cb}=\frac{m_c}{m_b}\,,\quad w_{cb}=\frac{1}{2}\left(z_{cb}+z_{cb}^{-1}\right)\,,\quad w_\pm(w)=w\pm\sqrt{w^2-1}\,, \tag{C.21}$$

$$r_w(w)=\frac{\log w_+(w)}{\sqrt{w^2-1}}\,, \tag{C.22}$$

$$\Omega_w(w)=\frac{w}{2\sqrt{w^2-1}}\Big[2\mathrm{Li}_2(1-w_-(w)z_{cb})-2\mathrm{Li}_2(1-w_+(w)z_{cb})$$

$$+\mathrm{Li}_2(1-w_+^2(w))-\mathrm{Li}_2(1-w_-^2(w))\Big]-wr_w(w)\log z_{cb}+1\,. \tag{C.23}$$

Here $\mathrm{Li}_2(x)=\int_x^0 dt\log(1-t)/t$ is the dilogarithm function and $V(\mu),T(\mu)$ are scale factors given as

$$V(\mu) \;=\; -\frac{2}{3}\big(wr_w(w)-1\big)\log\frac{m_bm_c}{\mu^2}\,, \tag{C.24}$$

$$T(\mu) \;=\; -\frac{1}{3}\big(2wr_w(w)-3\big)\log\frac{m_bm_c}{\mu^2}\,. \tag{C.25}$$

In our calculations we choose the scale $\mu = 4.2$ GeV. The $1/m_{b,c}$ corrections in eq. C.12 are given as

$$\delta\hat{h}_{V,m_b} = \hat{L}_1(w) - \hat{L}_4(w)\,, \tag{C.26}$$

$$\delta\hat{h}_{V,m_c} = \hat{L}_2(w) - \hat{L}_5(w)\,, \tag{C.27}$$

$$\delta\hat{h}_{A_1,m_b} = \hat{L}_1(w) - \frac{w-1}{w+1}\hat{L}_4(w)\,, \tag{C.28}$$

$$\delta\hat{h}_{A_1,m_c} = \hat{L}_2 - \frac{w-1}{w+1}\hat{L}_5(w)\,, \tag{C.29}$$

$$\delta\hat{h}_{A_2,m_b} = 0\,, \tag{C.30}$$

$$\delta\hat{h}_{A_2,m_c} = \hat{L}_3(w) + \hat{L}_6(w)\,, \tag{C.31}$$

$$\delta\hat{h}_{A_3,m_b} = \hat{L}_1(w) - \hat{L}_4(w)\,, \tag{C.32}$$

$$\delta\hat{h}_{A_3,m_c} = \hat{L}_2(w) - \hat{L}_3(w) + \hat{L}_6(w) - \hat{L}_5(w)\,, \tag{C.33}$$

$$\delta\hat{h}_{T_1,m_b} = \hat{L}_1(w)\,, \tag{C.34}$$

$$\delta\hat{h}_{T_1,m_c} = \hat{L}_2(w)\,, \tag{C.35}$$

$$\delta\hat{h}_{T_2,m_b} = -\hat{L}_4(w)\,, \tag{C.36}$$

$$\delta\hat{h}_{T_2,m_c} = \hat{L}_5(w)\,, \tag{C.37}$$

$$\delta\hat{h}_{T_3,m_b} = 0\,, \tag{C.38}$$

$$\delta\hat{h}_{T_3,m_c} = \frac{1}{2}\left(\hat{L}_6(w) - \hat{L}_3(w)\right)\,, \tag{C.39}$$

where the $\hat{L}(w)$ functions read

$$\hat{L}_1(w) = -4(w-1)\hat{\chi}_2(w) + 12\hat{\chi}_3(w)\,, \tag{C.40}$$

$$\hat{L}_2(w) = -4\hat{\chi}_3(w)\,, \tag{C.41}$$

$$\hat{L}_3(w) = 4\hat{\chi}_2(w)\,, \tag{C.42}$$

$$\hat{L}_4(w) = 2\eta(w) - 1\,, \tag{C.43}$$

$$\hat{L}_5(w) = -1\,, \tag{C.44}$$

$$\hat{L}_6(w) = -\frac{2(1+\eta(w))}{w+1} \tag{C.45}$$

The corrections of order $1/m_c^2$ are included via the subleading reduced IW functions $\hat{l}_{1-6}(w)$ as [40, 49]

$$\delta\hat{h}_{V,m_c^2} = \hat{\ell}_2(w) - \hat{\ell}_5(w)\,, \tag{C.46}$$

$$\delta\hat{h}_{A_1,m_c^2} = \hat{\ell}_2(w) - \frac{w-1}{w+1}\hat{\ell}_5(w)\,, \tag{C.47}$$

$$\delta\hat{h}_{A_2,m_c^2} = \hat{\ell}_3(w) + \hat{\ell}_6(w)\,, \tag{C.48}$$

$$\delta\hat{h}_{A_3,m_c^2} = \hat{\ell}_2(w) - \hat{\ell}_3(w) - \hat{\ell}_5(w) + \hat{\ell}_6(w)\,, \tag{C.49}$$

$$\delta\hat{h}_{T_1,m_c^2} = \hat{\ell}_2(w)\,, \tag{C.50}$$

$$\delta\hat{h}_{T_2,m_c^2} = \hat{\ell}_5(w)\,, \tag{C.51}$$

$$\delta\hat{h}_{T_3,m_c^2} = \frac{1}{2}\big(\hat{\ell}_3(w) - \hat{\ell}_6(w)\big)\,. \tag{C.52}$$

The IW functions are expressed, in general, as expansions about $w = 1$ as

$$f(w) = \sum_{n=0} \frac{f^{(n)}}{n!}(w-1)^n \tag{C.53}$$

with $f = \xi, \eta, \hat{\chi}_2, \hat{\chi}_3$ and $\hat{\ell}_i$. One can further relate the kinematic variable w with the expansion variable z as

$$w(z) = 2\left(\frac{1+z}{1-z}\right)^2 - 1. \tag{C.54}$$

One can then expand the IW functions up to any order in z as

$$f(w) = f^{(0)} + 8f^{(1)}z + 16(f^{(1)} + 2f^{(2)})z^2 + \frac{8}{3}(9f^{(1)} + 48f^{(2)} + 32f^{(3)})z^3 + ...(\text{higher orders}). \tag{C.55}$$

The authors of Ref. [48] have performed a simultaneous fit of the HQET parameters and the CKM element V_{cb} by considering an expansion of the IW functions up to order NNLO (3/2/1) and NNLO (2/1/0) where

$$\text{NNLO } (3/2/1): \quad \xi(w) \text{ up to } \mathrm{z}^3, \hat{\chi}_{2,3}(\mathrm{w}), \eta(\mathrm{w}) \text{ up to order } \mathrm{z}^2 \text{ and } \hat{\ell}_\mathrm{i} \text{ up to order z} \tag{C.56}$$

$$\text{NNLO } (2/1/0): \quad \xi(w) \text{ up to } \mathrm{z}^2, \hat{\chi}_{2,3}(\mathrm{w}), \eta(\mathrm{w}) \text{ up to order z and } \hat{\ell}_\mathrm{i} \text{ up to order } \mathrm{z}^0. \tag{C.57}$$

The fitted value of the parameters for the above two scenarios from Ref. [48] are given in Table C.2.

The other alternate way of parameterizing the form factors is due to Boyd, Grinstein and Lebed (BGL) [39]. It is similar to the CLN in the fact that they are both based on

the same dispersive bounds. However, unlike CLN, they do not employ HQET relations to reduce the number of FF parameters and are hence, more general. The form factors $\mathcal{F}_i \equiv \{f, g, \mathcal{F}_1, \mathcal{F}_2\}$ are expressed as series expansions in z as

$$\mathcal{F}_i(z) = \frac{1}{P_i(z)\phi_i(z)} \sum_{j=0}^{N} a_j^{\mathcal{F}_i} z^j, \tag{C.58}$$

where z is related to the recoil angle w as in Eq. (C.54) and $P_i(z) = \prod_p \frac{z-z_p}{1-zz_p}$ are called the Blaschke factors that help eliminate poles at $z = z_p$ at the B_c resonances given by

$$z_p = \frac{\sqrt{t_+ - M_p^2} - \sqrt{t_+ - t_-}}{\sqrt{t_+ - M_p^2} + \sqrt{t_+ - t_-}}; \quad t_\pm = (m_B \pm m_{D^*})^2. \tag{C.59}$$

The pole mass (M_p) for the different types of resonances are listed in Table C.3. The outer functions ϕ_i are given as

$$\phi_f = \frac{4r_{D^*}}{m_B^2} \sqrt{\frac{n_I}{6\pi\chi_{1^+}^T(0)}} \frac{(1+z)(1-z)^{3/2}}{\left[(1+r_{D^*})(1-z) + 2\sqrt{r_{D^*}}(1+z)\right]^4}, \tag{C.60}$$

$$\phi_g = 16r_{D^*}^2 \sqrt{\frac{n_I}{3\pi\tilde{\chi}_{1^-}^T(0)}} \frac{(1+z)^2(1-z)^{-1/2}}{\left[(1+r_{D^*})(1-z) + 2\sqrt{r}(1+z)\right]^4}, \tag{C.61}$$

$$\phi_{\mathcal{F}_1} = \frac{4r_{D^*}}{m_B^3} \sqrt{\frac{n_I}{6\pi\chi_{1^+}^T(0)}} \frac{(1+z)(1-z)^{5/2}}{\left[(1+r_{D^*})(1-z) + 2\sqrt{r_{D^*}}(1+z)\right]^5}, \tag{C.62}$$

$$\phi_{\mathcal{F}_2} = 8\sqrt{2}r_{D^*}^2 \sqrt{\frac{n_I}{\pi\tilde{\chi}_{1^+}^L(0)}} \frac{(1+z)^2(1-z)^{-1/2}}{\left[(1+r_{D^*})(1-z) + 2\sqrt{r_{D^*}}(1+z)\right]^4}. \tag{C.63}$$

The various relevant inputs for computing the outer functions are listed in Table C.4. The form factor coefficients $a_j^{\mathcal{F}_i}$ satisfy the weak unitarity constraints given by

$$\sum_{j=0}^{N} (a_j^g)^2 < 1, \quad \sum_{j=0}^{N} (a_j^f)^2 + (a_j^{\mathcal{F}_1})^2 < 1, \quad \sum_{j=0}^{N} (a_j^{\mathcal{F}_2})^2 < 1. \tag{C.64}$$

In addition to this, they are also subject to two kinematic constraints, one each at zero and maximum recoil respectively, given by :

$$\mathcal{F}_1(1) = m_B(1 - r_{D^*})f(1), \tag{C.65}$$

$$\mathcal{F}_2(w_{max}) = \frac{1 + r_{D^*}}{m_B^2(1 + w_{max})(1 - r_{D^*})r_{D^*}}\mathcal{F}_1(w_{max}). \tag{C.66}$$

In our analysis, we consider the fitted values of the form factor parameters from [14]. Lastly, for completion, we would like to list the relations between the BGL form factors and the hadronic form factors [51] :

$$g = \frac{2}{m_B + m_{D^*}}V, \tag{C.67}$$

$$f = (m_B + m_{D^*})A_1, \tag{C.68}$$

$$\mathcal{F}_1 = m_B(m_B + m_{D^*})(w - r_{D^*})A_1 - \frac{2m_B m_{D^*}(w^2 - 1)}{1 + r_{D^*}}A_2, \tag{C.69}$$

$$\mathcal{F}_2 = 2A_0. \tag{C.70}$$

The form factor dependences on q^2 for the various types of parameterizations are shown in Fig. C.1.

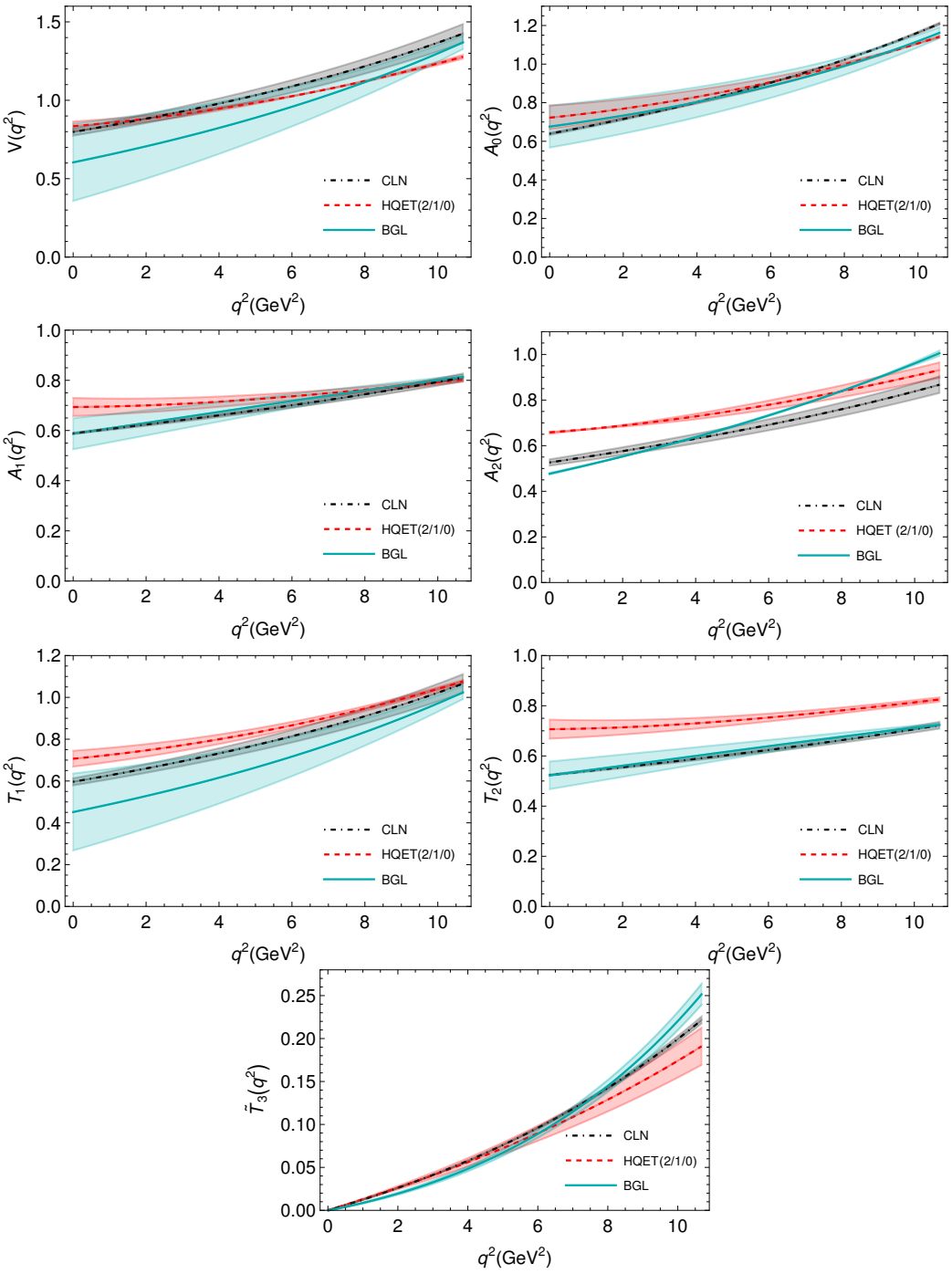

Figure C.1: Form factor dependence on q^2 for three different FF parametrizations. The shaded band show the region with the 1σ upper and lower limits of the form factor parameters listed in Tables C.1 and C.2 are considered without any correlation. For the HQET form factors, we show only the $2/1/0$ scenario following the analysis presented in Ref. [48]. Here, $\tilde{T}_3(q^2)$ is defined as $\tilde{T}_3(q^2) = T_3(q^2)q^2/(m_B^2 - m_D^{*\,2})$.

Parameter	HQET (3/2/1)	HQET (2/1/0)
$\xi^{(0)}$	1	1
$\xi^{(1)}$	-0.93 ± 0.10	-1.10 ± 0.04
$\xi^{(2)}$	$+1.35 \pm 0.26$	$+1.57 \pm 0.10$
$\xi^{(3)}$	-2.67 ± 0.75	$-$
$\hat{\chi}_2^{(0)}$	-0.05 ± 0.02	-0.06 ± 0.02
$\hat{\chi}_2^{(1)}$	$+0.01 \pm 0.02$	-0.06 ± 0.02
$\hat{\chi}_2^{(2)}$	-0.01 ± 0.02	$-$
$\hat{\chi}_3^{(0)}$	0	0
$\hat{\chi}_3^{(1)}$	-0.05 ± 0.02	-0.03 ± 0.01
$\hat{\chi}_3^{(2)}$	-0.03 ± 0.03	$-$
$\eta^{(0)}$	$+0.74 \pm 0.11$	$+0.38 \pm 0.06$
$\eta^{(1)}$	$+0.05 \pm 0.03$	$+0.08 \pm 0.03$
$\eta^{(2)}$	-0.05 ± 0.05	$-$
$\tilde{\ell}_1^{(0)}$	$+0.09 \pm 0.18$	$+0.50 \pm 0.16$
$\tilde{\ell}_1^{(1)}$	$+1.20 \pm 2.09$	$-$
$\tilde{\ell}_2^{(0)}$	-2.29 ± 0.33	-2.16 ± 0.29
$\tilde{\ell}_2^{(1)}$	-3.66 ± 1.56	$-$
$\tilde{\ell}_3^{(0)}$	-1.90 ± 12.4	-1.14 ± 2.34
$\tilde{\ell}_3^{(1)}$	$+3.91 \pm 4.35$	$-$
$\tilde{\ell}_4^{(0)}$	-2.56 ± 0.94	$+0.82 \pm 0.47$
$\tilde{\ell}_4^{(1)}$	$+1.78 \pm 0.93$	$-$
$\tilde{\ell}_5^{(0)}$	$+3.96 \pm 1.17$	$+1.39 \pm 0.43$
$\tilde{\ell}_5^{(1)}$	$+2.10 \pm 1.47$	$-$
$\tilde{\ell}_6^{(0)}$	$+4.96 \pm 5.76$	$+0.17 \pm 1.15$
$\tilde{\ell}_6^{(1)}$	$+5.08 \pm 2.97$	$-$

Table C.2: Values of input parameters needed for the HQET (3/2/1) and HQET (2/1/0) parameterizations of the hadronic form factors taken from [48].

Form Factor	Type	Pole Masses M_p (GeV)
g	1^-	$6.329, 6.920, 7.020$
$f, \mathcal{F}_1$	1^+	$6.739, 6.750, 7.145, 7.150$
$\mathcal{F}_2$	0^-	$6.275, 6.842, 7.250$

Table C.3: The pole masses corresponding to different types of B_c resonances as listed in [50].

Form Factor	Type
n_I	2.6
$\chi^T_{1^+}(0)$ GeV^{-2}	3.894×10^{-4}
$\tilde{\chi}^T_{1^-}(0)$ GeV^{-2}	5.131×10^{-4}
$\tilde{\chi}^L_{1^+}(0)$	1.9421×10^{-2}

Table C.4: Relevant inputs for the outer functions taken from [50].

VITA

B.S. in Physics, William & Mary (2020)

Cole-Eftnik Fellow (2020-present)